NTNU – Trondheim
Norwegian University of
Science and Technology

# Toxicity of cytostatic drug-loaded nanoparticles: The role of endocytosis.

**Trym Oliver Vogt**

Master of Science in Pharmacy
Submission date: June 2016
Supervisors: Siver Andreas Moestue
Tore-Geir Iversen

Norwegian University of Science and Technology
Faculty of Medicine. Department of Laboratory Medicine, Children's and Women's Health.

# Abstract

Poly alkyl cyanoacrylate nanoparticles have caught interest because of its desireable properties, such as biocompatibility and biodegradability. They are relatively easy to make and can entrap molecules which make them great drug carriers. With the expanding field of nanomedicine, understanding the properties of these drug carrier nanoparticles is of high importance if they are to be used in chemotherapy.

In this thesis cabazitaxel encapsulated in PIHCA nanospheres were used to study which mechanisms are involved in cellular uptake of the nanoparticle and the cytotoxic responses induced.

Cell viability tests were used to study whether or not endocytosis was involved in the toxicity of the drug encapsulated in nanoparticles. MTT and CellTiter-Glo ® assays were utilized to this extent. Confocal fluorescence microscopy was used to investigate cabazitaxel's effect on the cell cycle at various concentrations, the cells were marked with an fluorescent antibody for the cleaved form of PARP in order to study apoptotic cells. Results from these studies showed a reduction in the number of apoptotic cells and increase in the number of multinucleated cells with increasing concentrations of encapsulated cabazitaxel.

The cells showed some protection against the toxicity of drug-loaded nanoparticles using specific inhibitors of endocytic pathways. ATP depletion resulted in a 10-fold increase in protection against the toxicity of the encapsulated drug. Cell viability assays indicated that the drug-loaded nanoparticles are dependent on endocytosis to elicit a toxic effect. The results show that actin-dependent endocytosis might be important in the toxicity caused by encapsulated cabazitaxel.

# Acknowledgements

This master's thesis marks the end of my Master of Science program in Pharmacy at the Norwegian University of Science and Technology. The work with this thesis was carried out from August 2015 through May 2016 in Kirsten Sandvig's group at the Department of Molecular Cell Biology, Institute of Cancer Research at the Oslo University Hospital.

First of all I would like to thank my supervisor at the Molecular Cell Biology Department, Tore-Geir Iversen for giving me the opportunity to work on this exciting project. Thank you for all the advice, support and for always having the time to discuss experiments and results. Thank you for sharing of your knowledge of analytical methods and instruments. A final thanks for extra support, constructive feedback and critical review of my thesis. I would also like to thank Kirsten Sandvig for constructive input regarding my experiments and for the opportunity to do my master thesis in this group. I would also like to thank my internal supervisor at NTNU, Siver Moestue for great help regarding the more technical aspects of my master's thesis.

I would like to thank all the other members at the Molecular Cell Biology Department for being so welcoming and helpful at all times. The weekly meetings provided me with a lot of knowledge and were a great source for good feedback on my experiments. A special thanks to Anne for teaching me how to culture the HeLaDynK44A cell line, and to the workers at the cell lab for providing cultured cells for my experiments.

Thanks to my friends and family for supporting and believing in me throughout this work.

Trym Vogt

June 2016

# Table of contents

# Abbreviations

| | |
|---|---|
| ATP | Adenosine triphosphate |
| CIE | Clathrin-independent endocytosis |
| CLSM | Confocal laser scanning microscopy |
| CME | Clathrin-dependent endocytosis /Clathrin-mediated endocytosis |
| CTX | Cabazitaxel |
| cpm | Counts per minute |
| DMEM | Dulbecco's modified Eagle medium |
| DMSO | Dimethyl sulfoxide |
| DTX | Docetaxel |
| EE | Early endosome |
| EPR | Enhanced permeability and retention effect |
| FBS | Fetal Bovine Serum |
| LAMP-1 | Lysosomal-associated membrane protein 1 |
| LE | Late endosome |
| MDR | Multi-drug resistance |
| MPS | Mononuclear phagocyte system |
| MTT | 3-(4,5-dimethylthiazol-2-yl)-2,5-diphenyltetrazolium bromide |
| MVB | Multivesicular body/endosome |
| NADH | Nicotinamide adenine dinucleotide |
| nm | Nanometer |
| PACA | Poly (alkyl cyanoacrylate) |
| PBS | Phosphate buffered saline |
| PEG | Poly (ethylene-glycol) |
| PIHCA | Poly (Isohexyl cyanoacrylate) |
| rpm | rotations per minute |
| Tet + | Cells of the HeLaDynK44A cell line in the presence of tetracycline |
| Tet - | Cells of the HeLaDynK44A cell line in the absence of tetracycline |
| VEGF | Vascular endothelial growth factor |

# 1 Introduction

Nanomedicine is a relatively young discipline in the field of medicine, it entails the use of nanotechnology for diagnosis, imaging, monitoring and treatment of the human body. Nanoparticles currently in clinical use are utilized as vehicles for drug delivery, improving drug half-life, targeting the nanoparticles to specific organs to optimize therapeutic effect and reduce adverse reactions in other organs, as well as diagnostics and *in vivo* imaging [1-3].

Nanoparticles can be administered through different routes, including oral, dermal, rectal, inhalation, nasal or parenteral. Most nanoparticle-based drug formulations on the market today are administered parenterally [5]. When nanoparticles enter the blood stream they are immediately exposed to various proteins, some of these proteins adsorb to the surface of the nanoparticle and form a "corona" around the particle. Some of these proteins, such as immunoglobulin G, are called opsonins, they "tag" the nanoparticles so that they are more easily targeted by macrophages. Nanoparticles bound with many such proteins tend to concentrate in the liver and spleen where the cells of the mononuclear phagocyte system (MPS) are most abundant. Other proteins, such as albumin, are so called dysopsonins, this makes the particle less likely to interact with cells. Nanoparticles bound with many dysopsonins have a prolonged circulation in the blood. To reduce the amount and types of protein bound on the nanoparticle surface some nanoparticles are made with a coating. This coating is usually a polymer such as polyethylene glycol (PEG) or a polysaccharide. PEGylation has been shown to reduce interaction between different nanoparticles and blood proteins and helps avoid recognition by the MPS, thus prolonging the particle's circulation time [6].

Nanoparticles are used in anticancer treatment because they provide a method of targeted delivery that is impossible with small-molecule drugs. There are active and passive targeting mechanisms that allow delivery of nanoparticles to the site of action. Passive targeting is when nanoparticles accumulates at the desired site of action just by being in systemic circulation over time. This occurs in tumor tissue due to the enhanced permeability and retention (EPR) effect. When tumors reach a certain size the cancer cells start to secrete VEGF to induce angiogenesis. These blood vessels, formed in and around a growing tumor, are dilated, irregulary shaped and the endothelial cells are disorganized. This causes large gaps in the vasculature which in turn

causes leakage of blood plasma components. These kind of defective blood vessels are not found elsewhere in the body. Nanoparticles in the blood stream will circulate until they leak out of these enlarged gaps and accumulate in tumor tissue [7].
Active targeting is when the nanoparticles have certain qualities, such as surface functionalization with ligands that specifically targets the desired tumor site. Many cancer cells overexpress certain receptors and surface proteins, and thus are ideal targets for nanoparticles that recognize these receptors or proteins. This ensures that the nanoparticles accumulate and interact more efficiently in tumor tissue than elsewhere in the body [7].

## 1.1 Nanoparticles

Though few nanoparticles are currently approved for clinical use in humans, the number of nanoparticle based drugs in development is increasing rapidly. Some of these nanomedicines may potentially become a nanoparticle based therapeutic or diagnostic tool. There are quite few nanoparticle based therapeutics on the market, they are used for targeted drug delivery and diagnostics [2, 8]. Among those currently on the market are liposomes (Doxil ®), Albumin-bound drugs (Abraxane ®) and PEGylated proteins (PEGASYS ®, Neulasta ®).

Nanoparticles have been defined as having one dimension smaller than 100 nm [9]. However, some nanoparticles are of larger size and with various shapes. Some nanoparticles have been found to be ideally sized between 50-200 nm [10]. A feature of nanoparticles is that they have a very large surface area per weight, this means that they intrinsically have a great potential to interact with other objects in the body [9].
Nanoparticles are usually divided into two categories, organic, also called soft, and inorganic, also called hard, based on their composition. Soft nanoparticles include liposomes, dendrimers and polymeric particles. Liposomes are vesicles with a lipid bi-layer of phospholipids and an aqueous core. This enables them to efficiently carry hydrophilic drugs in the core or hydrophobic drugs in the lipid bi-layer. Because they are composed of phospholipids, liposomes are biocompatible, meaning they do not cause allergic or immunologic responses. However they are vulnerable to clearance via the MPS [11]. Dendrimers are complex structures of branched units originating from a central core. Dendrimers can have different functionalities based on the type of dendrimer used and the morphology. The tree-like structure of dendrimers gives the particle a range of reactive site inside the particle and on the surface. The internal cavities can be used to encapsulate drugs, while the reactive terminal groups can be modified

for targeting and diagnostics puposes [11]. Polymeric nanoparticles are a group of nanoparticles that consists of nanospheres and nanocapsules, among others. Polymeric nanoparticles can be made of several different polymers including synthetic polylactides, poly(phosphoesters), polyanhydrides and poly(alkyl cyanoacrylates) (PACA), but also natural polymers like polysaccharides, chitosan and dextran [4]. Nanocapsules are a two-phase system consisting of a homogenous polymeric shell with a hydrophobic or aqueous core that can be loaded with drugs or fluorescent dyes. Nanospheres are solid polymeric matrices that can be loaded with drugs by dispersion inside the matrix, adsorption on the surface or conjugated to the polymer [4, 12].

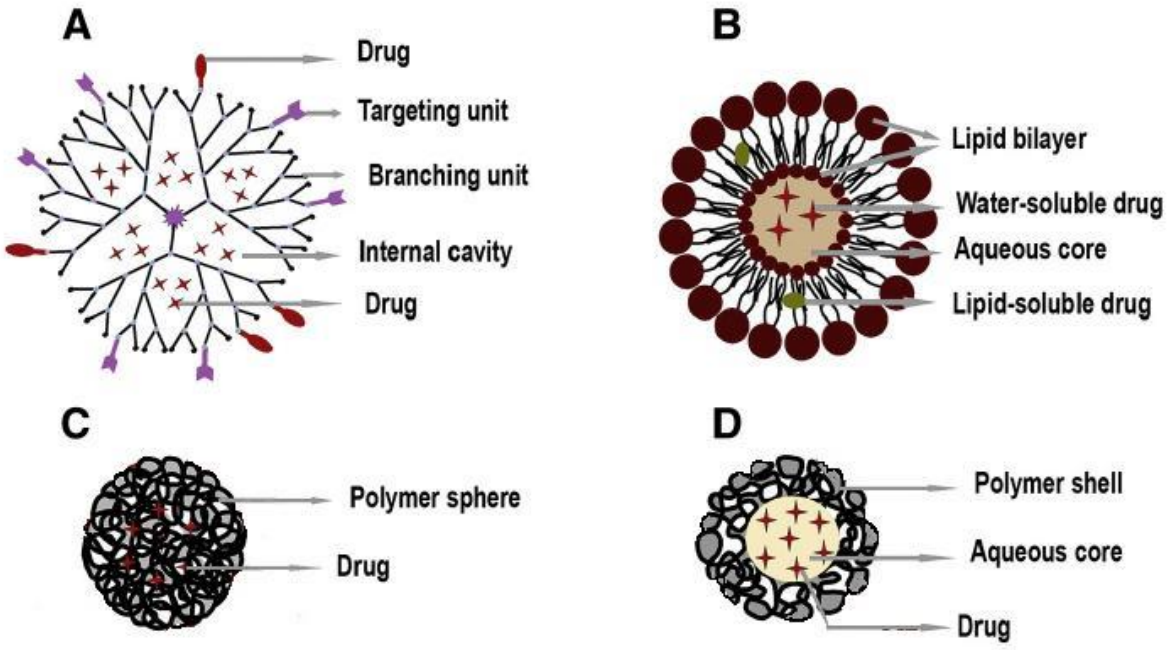


**Figure 1.1. Structure of soft nanoparticles including denrimer (A), liposmes (B), polymeric nanosphere (C) and polymeric nanocapsule (D). Illustration adapted from [11].**

Hard nanoparticles include quantum dots and metal oxides. Quantum dots are characterized by a solid crystal core of semiconducting metal. The core gives the particles unique fluorescent properties [2]. Because of this quantum dots are used mainly for imaging purposes [11]. Metal oxide nanoparticles have properties that make them highly usable for imaging. Iron oxide particles have long been used as contrast agents for MRI. More recently, manganese oxide particles started being used for this as well as it gives a different contrast [2]. Another type of metal oxide nanoparticle is the superparamagnetic iron oxide nanoparticle (SPION), they

produce higher contrast per particle, thus reducing the amount needed for MRI-imaging and reducing toxicity. Metal oxide nanoparticles have metallic cores [11].

The surface of nanoparticles may be coated with polymers or polysaccharides to modify the particle's surface charge, biocompatibility, biodegradability and targeting properties. Some of the substances used are PEG, poloxamer, polysorbate and dextran, of which PEG is preferred [6]. PEG has a basic structure of polyether with hydroxyl groups attached to each end:

$$HO–(CH_2CH_2O)_n–CH_2CH_2–OH.$$

The length of the polymer is variable and the effect of PEGylation depends on the length of the PEG polymer [10].

In this master thesis, poly (isohexyl cyanoacrylate) (PIHCA), a type of PACA nanoparticle, was used to determine to which extent endocytosis of the nanoparticles affects the cytotoxicity of the encaspulated drug. The size of the particles used in this thesis varied between 130 nm and 180 nm. A schematic representation of a PACA and potential loading is shown in figure 1.2.

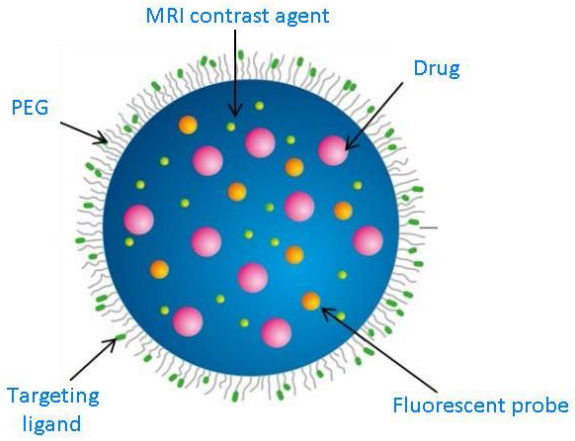


**Figure 1.2. Schematic of a PACA nanosphere. Illustration from presentation by Ruth Schmid, SINTEF.**

### 1.1.2 Synthesis of PACAs

Monomers of PACA polymerize easily in presence of water or nucleophiles and an initiator is rarely necessary. There are two types of preparation methods used to synthesize PACAs, the first is through polymerization of monomers, and the second is through dispersion of a preformed polymer [13]. An overview of these preparation methods is shown in figure 1.3.

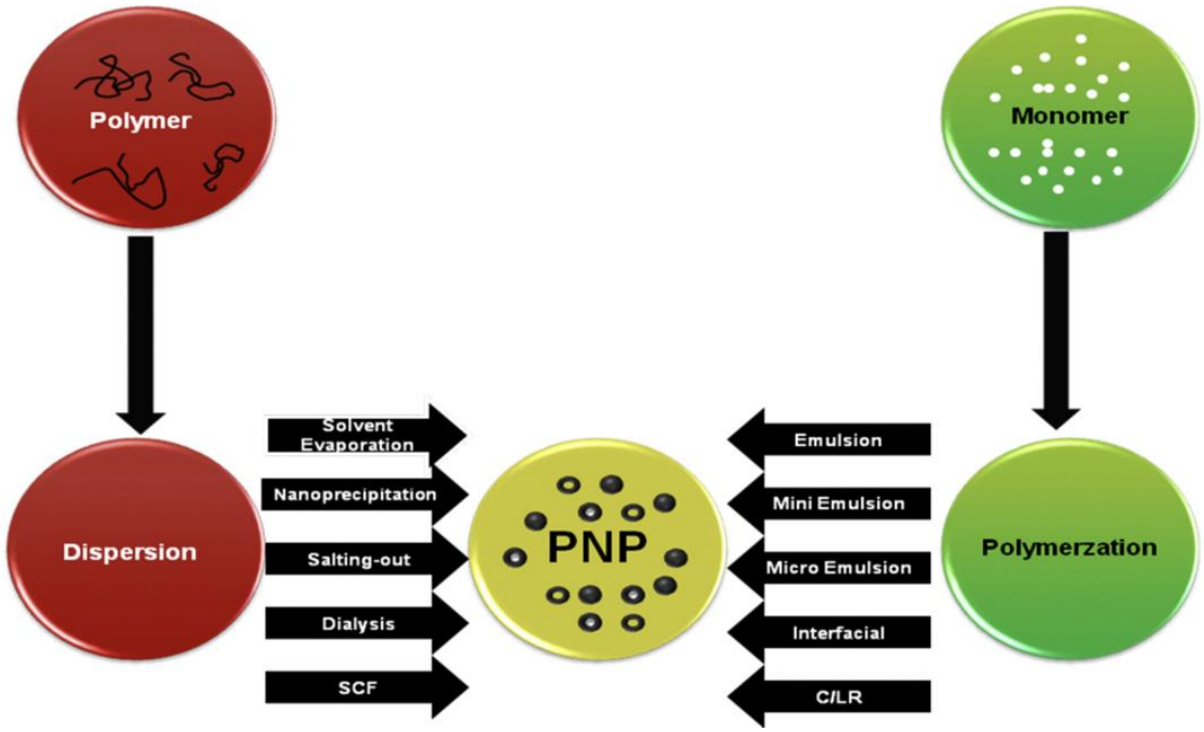


**Figure 1.3. Different methods for preparation of PACA nanoparticles. From [Rao, Geckeler].**

The PIHCA nanoparticles used in this thesis were prepared using the miniemulsion method. In this process the monomer and the drug or dye to be encapsulated are kept in an organic phase, while the aqueous phase contains surfactants, if any are to be used. Because of the alkyl cyanoacrylates' high reactivity to nucleophiles the aqueous phase should be acidic [14].

The two phases are homogenized using a high-shear device and an initiator starts the polymerization. As previously noted, alkyl cyanoacrylates undergo anionic polymerization, thus adding sufficient NaOH to the acidic aqueous phase will initiate the reaction [13].

## 1.2 Endocytosis and intracellular transport

Endocytosis is the main mechanism cells use for uptake of nutrients from the extracellular environment. This is essential in all cells in the body because most of these nutrients and other substances the cells need are polar and will not pass through the cell membrane by diffusion or other forms of passive transport. Endocytosis is also important in other physiological and cellular processes, including intra- and intercellular communication, neurotransmission, regulation of cell surface proteins, receptors and transporters and uptake of large particles such as bacteria [15, 16]. There are several mechanisms of endocytosis including phagocytosis, macropinocytosis, clathrin-mediated endocytosis (CME) and clathrin-independent endocytosis (CIE). Further, they can be divided into dynamin-dependent and dynamin-independent endocytosis.

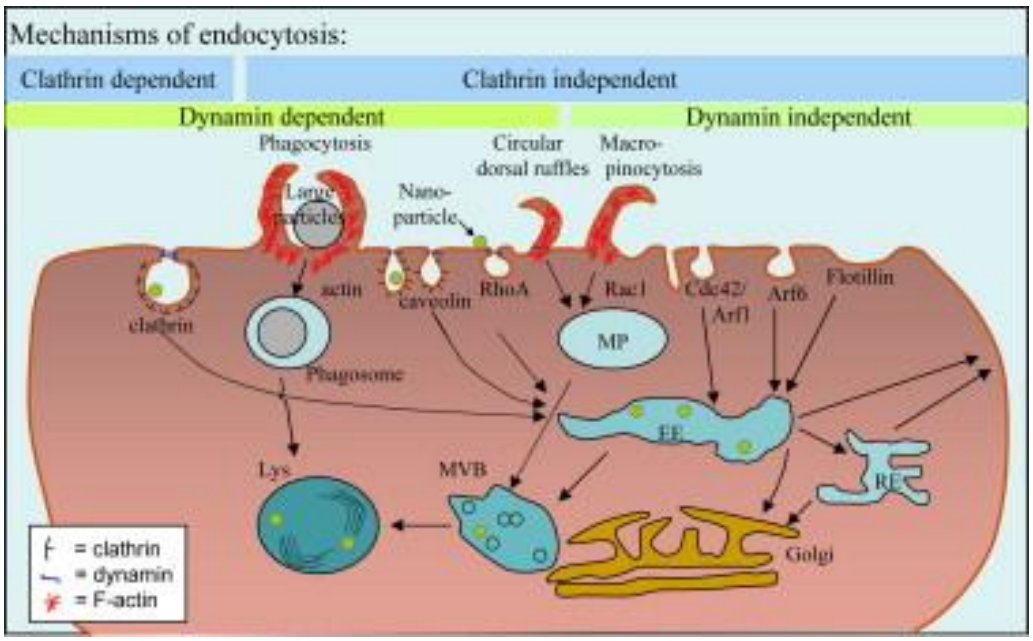


**Figure 1.4. Illustration of endocytic mechanisms. From [16].**

**Phagocytosis**, also referred to as "cell eating", is the mechanism in which a cell ingests solid particles, including particles >500 µm, such as bacteria. Phagocytosis is the main weapon of the MPS and is used to remove pathogens from the body, but also remove debris from apoptotic cells in tissue. Initial contact between a particle and the plasma membrane may lead to further interactions, such as via receptors. This stimulates the cell to assemble actin filaments that form protrusions that engulf the particle, subsequently internalizing it into phagosomes. In the

cytosol phagosomes fuse with lysosomes and form phagolysosomes where the particle is degraded [15].

**Macropinocytosis** is a mechanism employed by all cells. The process is also called "cell drinking", this is because it is a non-selective uptake of extracellular fluid. Changes in the actin cytoskeleton cause the plasma membrane to form ruffles which protrude and envelop fluid and any nutrients it contains. The contents are then internalized in vacuoles [16].

**Clathrin-dependent endocytosis** (CME) is the most studied form of endocytosis. CME is a very versatile pathway with functions including regulating surface expression of proteins, controlling activation of signaling pathways, turnover of membrane components and uptake of nutrients. In response to stimuli the plasma membrane forms an invagination, also referred to as a pit, clathrin is recruited and coats the pit from inside the cell. The pit then expands and form a vesicle which is then pinched off by the GTP-ase dynamin. The clathrin coated pits form vesicles in sizes between ~35-42 nm, however there have been reported sizes up to 200 nm. Endocytosis of these larger cargoes often employs a combination of clathrin and actin to coat the pit before it can be internalized [17].

**Clathrin-independent endocytosis** (CIE) is the final category of endocytosis and includes a variery of mechanisms. CIE is divided into two distinct classifications, dynamin-dependent and dynamin-independent. Dynamin-dependent mechanisms include RhoA/Rac1 and caveolin-caveolae/lipid raft. RhoA/Rac1 dependent endocytosis utilizes actin in the endocytosis of cargo, including the interleukin-2 receptor [18]. Dynamin-independent mechanisms include Cdc42 and Arf6. Flotilins have been found to be involved in endocytic mechanisms in both dynamin-dependent and dynamin-independent endocytosis [19].

After endocytosis via the CME or CIE mechanisms vesicles are formed which contain the endocytosed cargo. These vesicles then fuse with the early endosome (EE) where a slightly acidic environment (pH ≈ 6) causes dissociation of certain complexes. Membrane lipids and receptors are then selectively isolated and recycled back to the plasma membrane of the cell via recycling endosomes [20, 21]. The EE, with the remaining cargo, matures into- or pinch off a smaller part to form a multivesicular endosome (or multivesicular body, MVB) [22]. These MVBs are then translocated along microtubules and fuse with late endosomes (LE). LE plays an important part in sorting the endocytosed cargo, some proteins are cycled to the Golgi apparatus, while other contents are destined for further degradation [22]. LE will eventually fuse with lysosomes, which causes a further reduction in pH (pH ≈ 5) and the addition of high

concentrations of lysosomal enzymes, this will result in the degradation of most substances [20, 21].

## 1.3 Degradation of PACA

There are different degradation pathways for PACAs described in literature. One mechanism is that the ester bond of the alkyl side chain is hydrolyzed, resulting in an alkylalcohol and poly(cyanoacrylic acid). This reaction can be catalyzed by esterases in serum and lysosomes. The time it takes for the polymer to be degraded this way varies with the side chain length, but will be a couple of hours. Another mechanism of degradation is an inverse Knoevenagel reaction. This reaction occurs passively in water at physiological pH. The reaction cleaves the polymer and yields formaldehyde and cyanoacetic esters [13]. The rate of degradation is dependent on the alkyl side chain [23].

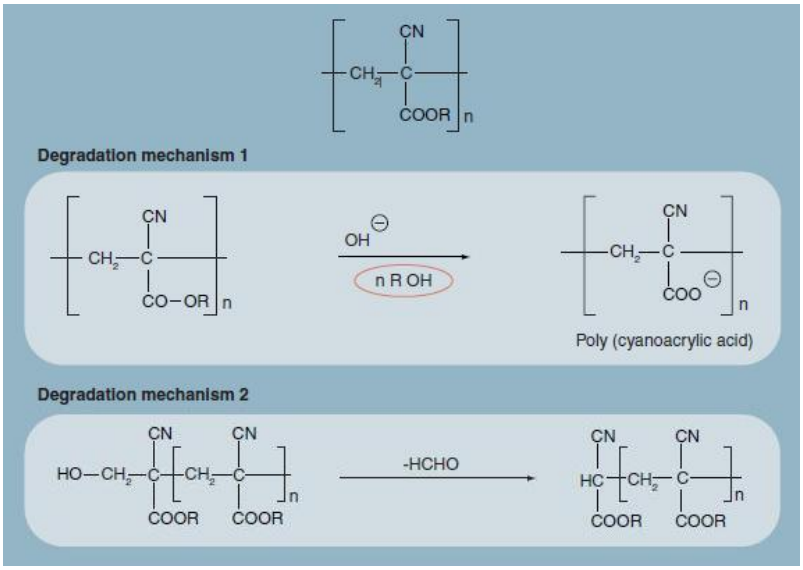


**Figure 1.5. Different mechanisms of degradation.**
**Illustration adapted from [4].**

Cytotoxicity of nanoparticles is an important facet of their properties, and is highly relevant because they are often endocytosed in cells. PACAs have been reported to cause different mechanisms of cytotoxicity. The first is cytotoxicity of degradation products released from the polymer. The second is release of inflammatory mediators from the cells as a result of contact and stimulation by the nanoparticles. The third mechanism reported is caused by adhesion of nanoparticles on the cell membrane, which results in interactions that can compromise the cell

membrane [13]. The toxicity of PACAs show varying degrees of toxicity based on the degradation rate of the polymer [23].

## 1.4 Cytotoxicity of chemotherapeutic agents

Ever since the first successful transplantation of tumor models into animals there have been extensive developments of chemotherapeutic agents. When studying chemotherapeutics it is necessary to first understand how they interact with the cells.

Cancerous cells, like their healthy originators, need to divide in order to fill any space left by dead cells. Cancerous cells divide faster than healthy cells and if left unchecked will increase the size of the tumor indefinitely. The cell cycle is the process in which a cell divides, and it is divided into four phases, $G_1$, S, $G_2$ and M.

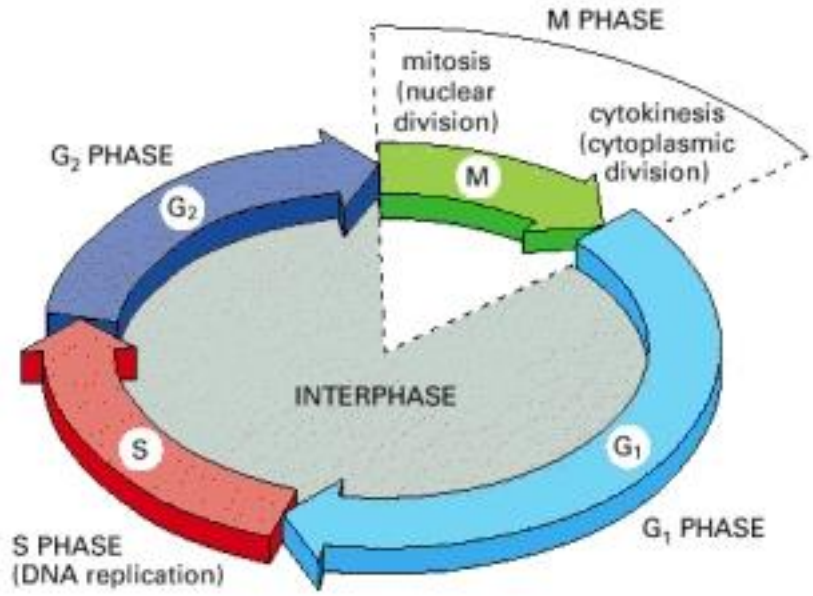


**Figure 1.6. The phases of the cell cycle. Illustration from [24].**

The $G_1$ phase is the phase in which the cells grow in size and maintains protein synthesis and renewal of organelles. In this phase the cell monitors the extracellular environment and, if deemed favorable, progresses to S phase. In the S phase the cell synthesizes a second set of DNA. Following S phase is $G_2$, in which the cells continue to grow and monitors the extracellular environment before it can proceed to the M phase. In the M phase the DNA is packed into compact chromosomes. Mitosis is the process in M phase that marks the division

of the cell's nucleus, the two nuclei are moved to each end of the dividing cell. When this is complete the cell pinches in two by cytokinesis and the cell division is complete [24].

The first taxane, taxol was isolated in 1971 [25]. When other taxanes were discovered taxol was renamed paclitaxel. Paclitaxel finally received FDA approval in 1992, followed by another taxane, docetaxel, in 1999 [26].
Taxanes inhibit the depolymerization of microtubules in the cells. Taxanes has also been found to enhance and promote nucleation and elongation during microtubule polymerization, resulting in abnormal microtubulin formation. This disrupts several functionalities within the cells [27]. During the cell cycle microtubules is used to form a mitotic apparatus which is necessary for separation of the two sets of chromosomes and also makes a spindle between the two halves of the dividing cell. After the translocation of one set of chromosomes to each pole of this mitotic spindle the cells need to break apart the spindle to enable scission of the cells [28]. When the cells are unable to break down the microtubules, the cell cycle will be arrested. Mitotic arrest often results in cell death, but may also result in mitotic slippage and formation of multinucleated cells [27]. The exact mechanisms of cell death induced by taxanes have not been concluded, however mitotic catastrophe and apoptosis have been observed. Taxanes have been seen to induce activation of caspase-3 and a subsequent cleavage of its substrate, PARP, resulting in apoptosis [29].

Most of the experimental work in this thesis was done with cabazitaxel. Cabazitaxel was developed and approved in 2010 as a treatment for castration-resistant prostate cancer in patients who had developed resistance to docetaxel [30]. Despite having a similar mechanism of action to paclitaxel and docetaxel, cabazitaxel has a distinctly different molecular structure than its predecessors. This difference in structure gives cabazitaxel a low affinity for the the ATP-dependent efflux pump P-glycoprotein, which is associated with anti-tumor drug resistance [31].

## 1.5 Experimental techniques

### 1.5.1 Cell proliferation

Cell proliferation is the result of cell growth and cell division. Cancer cells are defined by their ability to proliferate rapidly and with minimal apoptosis. Thus, when studying chemotherapeutic drugs, cell proliferation is a well suited marker for determining the efficacy

of the treatment. For studying cell proliferation there are different types of assays that can be used, including counting the number of cells, measuring metabolic activity of the cells, determining the amount of DNA synthesized in the cells or measuring the concentration of adenosine triphosphate (ATP) in the cells [32].

### 1.5.2 Metabolic activity

Many experiments in this thesis use the MTT assay for cell viability. MTT is a colorimetric assay that is used as an indirect method for measuring metabolic activity. In living cells MTT is reduced by the coenzyme NADH, resulting in insoluble formazan, which is a purple-colored dye. To properly quantify the formazan produced by this reaction in the living cells, the insoluble salts have to be solubilized, this is normally done using DMSO [33].

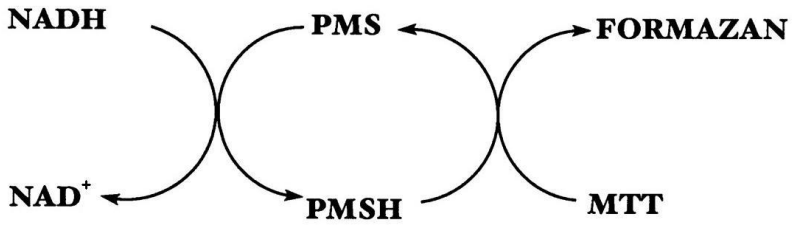


**Figure 1.7. Indirect reduction of MTT to formazan by NADH.**

For other experiments the CellTiter-Glo® viability assay was used. CellTiter-Glo is a luminescence-based assay and generates a luminescence proportional to the amount of ATP present in the cells which indicates the presence of metabolically active cells.

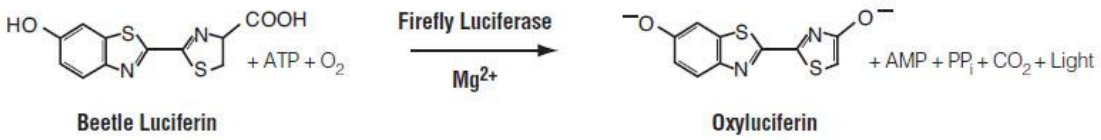


**Figure 1.8. CellTiter-Glo® reaction formula. From [34].**

### 1.5.3 Fluorescence and Confocal Laser Scanning Microscopy

Fluorescence is the process in which a molecule absorbs energy from light by excitation of electrons and emits light. The emitted light has a lower wavelength; this is due to a loss of energy in the molecule which causes the emitted light to have lower energy.

Some experiments in this thesis was done using confocal laser scanning microscopy (CLSM), which is a technique used for imaging living or fixed cells. The cells are marked with fluorescently labeled substances that have affinity for certain proteins in the cell that are of interest to study. CLSM is often preferred over normal fluorescence microscopy because it is able to block out light that is out of focus, this is done by use of pinholes as shown in figure 13. The laser passes through a pinhole and is reflected by a mirror after which an objective focuses the light to a point inside or on the surface of the sample. The laser beam then excites the fluorophores in the sample and the emitted light is focused by the objective lens and passes through a beam splitter that allows the beams of emission wavelength pass but blocks the excitation wavelengths. Then the emitted light passes through another pinhole and is detected and subsequently translated to electrical signals and recorded by a computer.

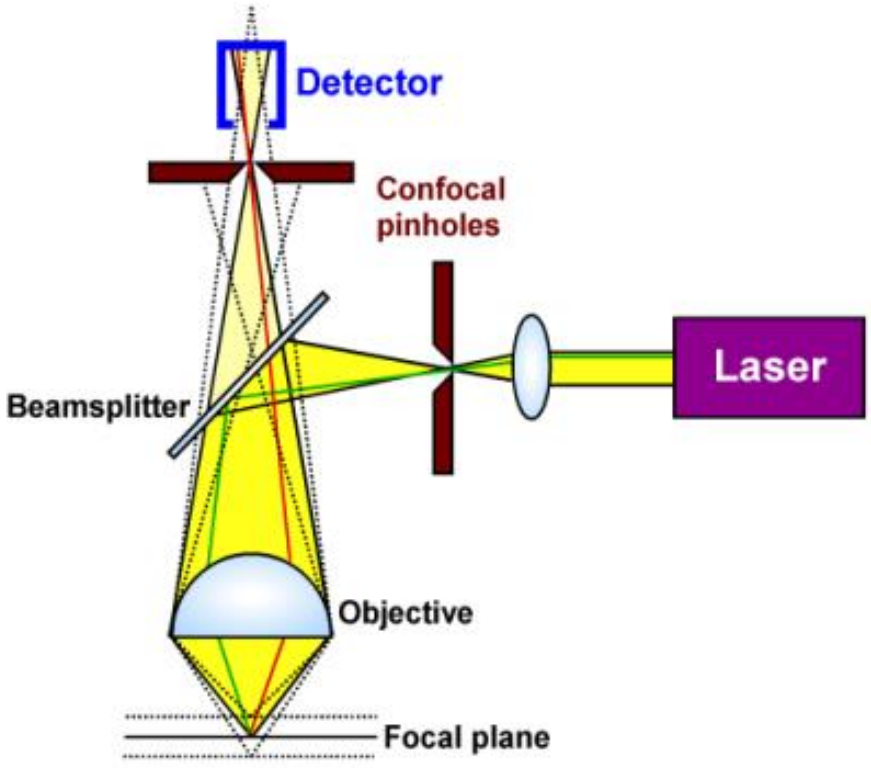


**Figure 1.9. Schematic showing the optical principle of confocal laser scanning microscopy. Image from [35].**

# 2 Materials and methods

## 2.1 Cell lines

To use a cell line in experiments, they need to be cultured in growth media with all the essential nutrients; amino-acids, vitamins, metals, minerals, salts, glucose, glutamine, pH-buffers, fetal bovine serum (FBS) and antibiotics. FBS is a normal addition to growth media as this provides a variety of proteins, hormones, growth factors, lipids and cytokines. The antibiotics normally added to growth media are penicillin and streptomycin, which are added to inhibit microbial growth in the media. Most growth media also contains a pH-indicator, most often phenol red. Phenol red is red at physiological pH and changes towards yellow when pH decreases and towards purple when pH increases. All cell cultures were grown at 37°C with 5% $CO_2$ and $H_2O$- saturated air. Growth media is buffered with sodium bicarbonate and 5% $CO_2$ is necessary to maintain physiological pH. Three different cell lines were used in the experiments: HeLaP, HeLaDynK44A and MDA-MB-231.

**Table 2.1. Cell lines.**

| Cell Line | Species | Cell Type | Derived from |
|---|---|---|---|
| **HeLa** | Human | Epithelial | Cervix carcinoma |
| **MDA-MB-231** | Human | Epithelial | Breast adenocarcinoma |

The HeLaP cell line was cultured in DMEM supplemented with 10% FBS and 1% penicillin and streptomycin. The HeLaDynK44A cell line was cultured in DMEM supplemented with 10% FBS, 1% penicillin and streptomycin, 400 µg/ml G418 (Geneticin®) and 200 ng/ml puromycin aswell *as 1%* tetracycline. DMEM is a liquid medium that contains glucose, L-alanyl-glutamin and a sodium bicarbonate-buffer. The MDA-MB-231 cell line was cultured in RPMI medium supplemented with 10% added FBS and 1% penicillin and streptomycin. RPMI is a liquid medium that contains L-alanyl-glutamin and a sodium bicarbonate-buffer. Some experiments with the HeLa cell line also necessitated the use of Hepes-buffered medium. Hepes is a buffer that is more efficient in maintaining physiological pH in environments with

fluctuations in $pCO_2$, than bicarbonate-buffers. Unless otherwise noted the cell lines were incubated with their respective culture media during experiments.

## 2.2 Nanoparticles

The PIHCA nanoparticles used in this thesis were supplied by SINTEF materials and chemistry. The nanoparticles were loaded with cabazitaxel (CTX), docetaxel (DTX) or cabazitaxel and NR668, a modified variant of the fluorescent dye Nile Red. NR668 is a highly lipophilic dye and is therefore unlikely to leak out of the lipophilic PIHCA sphere [36]. NR668 has an excitation and emission maxima at 561 nm and 630 nm. The nanoparticles used in this thesis and their properties are shown in table 2.2.

**Table 2.2**

| Particle | Monomer | PEGylation | Size (nm) | Encapsulated substance (% w/w) |
|---|---|---|---|---|
| **BBB-31** | IHCA | Pluronic F68 & Kolliphor HS15 | 160 | Cabazitaxel (5.4%) |
| **BBB-34B** | IHCA | Pluronic F68 & Kolliphor HS15 | 180 | - |
| **NC-103** | IHCA | Pluronic F68 & Kolliphor HS15 | 136 | Cabazitaxel (9.7%) NR668 |
| **NanoCan-48** | IHCA | Pluronic F68 & Kolliphor HS15 | 167 | Docetaxel (1.7%) |

## 2.3 Fluorescence microscopy studies

The confocal laser scanning microscope Zeiss LSM 780 (Carl Zeiss Jena GmbH, Germany) was used for acquiring fluorescence images. A 63x oil based objective was used. Confocal images acquired were processed using the Zeiss LSM Image Browser software (version 4.2.0.121). Images were acquired with the pinhole set to 1 AU, which corresponds to 0.7 µm for all fluorescent substances.

Two fluorescence microscopy studies were performed in the work of this thesis. A colocalization study between lysosomes and the nanoparticles loaded with NR668 was

performed to determine the extent of endocytosis at concentrations where the loaded drug elicits a toxic response. For this experiment an antibody for Lysosomal-associated-membrane-protein 1 (LAMP-1) was used. A qualitative study of cell death mechanisms was also performed to observe which drug concentrations that induce cell death and if apoptosis is the most frequent mechanism of death. For this experiment, an antibody for the cleaved form of Poly (ADP-ribose) polymerase (PARP) was used.

**Experimental procedures**

For the microscopy studies HeLaP cells were seeded out the day prior to the experiments in 4-well plates with one cover slip in each well with a density of $4x10^4$ cells/well in 1 mL medium. Drug-loaded PIHCA, with or without NR668, was then added in concentrations of 1, 10, 100 or 1000 nM of CTX to each well. The plates were then incubated for 4 hours. The PIHCAs were then washed off and the plates were either fixed in 4 % paraformaldehyde (PFA), or chased for 24 or 48 hours before fixation and subsequent immunostaining steps.

For immunostaining, the cells were washed with medium at 37°C, followed by PBS (isoton sodium chloride, buffered with phosphate to pH 7.4) to remove nanoparticles not bound to the cells. The cells were then fixed using a 4% paraformaldehyde solution for 15 minutes at room temperature. The cells were then washed twice with PBS and incubated in blocking buffer (PBS with 0.1% saponin and 2% bovine serum albumin) for 1 hour at room temperature.

For colocalization studies between the PIHCA particles and lysosomes in HeLaP and MDA-MB-231, the primary antibody anti-LAMP-1 (rabbit) was used together with the secondary fluorophore conjugated antibody Alexa488 (donkey anti-rabbit).

For the toxicity studies to see whether PIHCA induced apoptosis in HeLaP cells, the primary antibody anti-PARP1 (cleaved form, rabbit) was used together with the secondary fluorophore conjugated antibody Alexa488 (donkey anti-rabbit).

The primary antibodies were diluted in blocking buffer and one drop was spotted onto each cover slip. The plates were then incubated for 1 hour at room temperature. The cover slips were then washed twice for 10 minutes with PBS and once for 10 minutes in blocking buffer. The secondary antibodies were diluted in blocking buffer and spotted onto each cover slip and incubated in the dark, at room temperature for 30 minutes. The cover slips were then washed twice for 10 minutes with PBS and once for 10 minutes in blocking buffer. The cover slips were briefly washed in MilliQ water and carefully dried prior to mounting with ProLong

Gold with DAPI on objective slides. The samples on objective slides were then incubated in refrigerator for 24 or 72 hours. The samples were inspected using confocal fluorescence microscopy.

## 2.4 Toxicity and endocytosis studies

Different mechanisms of endocytosis can possibly be involved in the cellular uptake of nanoparticles. Which pathways are used by a cell is different for various cell-lines and may vary between nanoparticles of different size, charge and other physicochemical properties. Various pharmacological inhibitors are often used to block different endocytic pathways. However, one should be aware that many of the inhibitors are not very specific. Inhibiting one of these endocytosis pathways may induce up-regulation of other pathways. Endocytosis of nanoparticles in itself can cause a change in cellular responses such as malfunctioning of the lysosomal system, down-regulation of growth factor receptors and changes in the membrane recycling [16]. The experiments were executed in an incubator at 37°C and with 5% $CO_2$, unless otherwise stated.

**Dynamin dependent endocytosis**

To investigate if dynamin-dependent pathways of endocytosis are involved in the uptake of PIHCA nanoparticles the cell line HeLaDynK44A was used.

The HeLaDynK44A cell line has a tetracycline-inducible system for expression of a dominant-negative dynamin-1 mutant. A tetracycline-inducible system is a way to control the activation of a specific gene. The Tet-Off system used in this cell line consists of a tetracycline-Controlled Trans-Activator protein (tTA) which binds to Tetracycline-operator (Tet-op) sequences in the promoter-region of the target gene. The tTA is created by fusion of the Tetracycline repressor protein found in *Escherichia coli* and the activation domain of the VP16 protein found in *Herpes simplex virus*. With tetracycline present, the tetracycline binds to the tTA and prevents its binding to Tet-op sequences, thereby hindering expression of the target gene [Gossen et al]. The target gene in question in the HeLaDynK44A cell line is a mutated dynamin gene that, when expressed, effects the production of dysfunctional dynamin. This will in turn disrupt dynamin-dependent endocytosis.

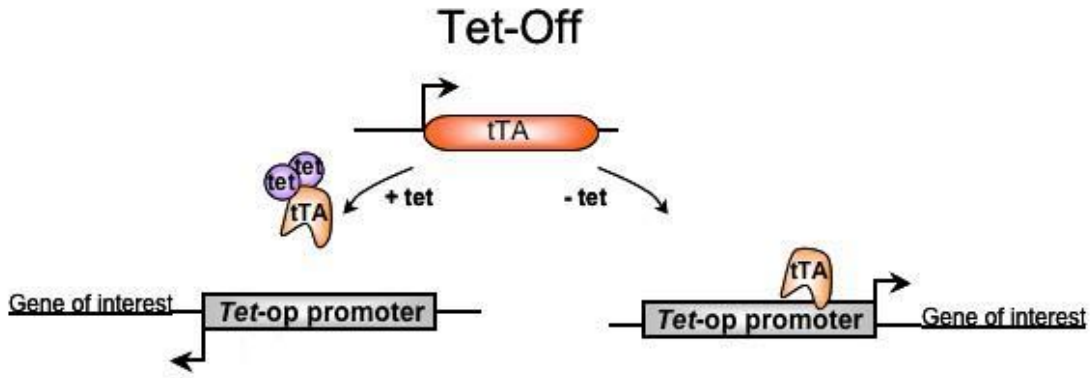


**Figure 2.1. Illustration of the Tet-Off system. Image adapted from [37].**

In other experiments Dyngo 4a was used to inhibit dynamin function. Dynamin is an essential part of several endocytosis pathways (figure 1.6), including CME [38]. Dynamin has also been shown to be part of some CIE mechanisms [18, 39].

**CIE and macropinocytosis**

CK-666, an inhibitor of the actin related protein 2/3 (arp2/3) complex and latrunculin B, an inhibitor of actin polymerization, were used to block some mechanisms involved in CME, CIE and macropinocytosis [16-18, 39]. The experiments using these inhibitors were done in media without serum, Dyngo has been shown to be 10-fold less potent in the presence of even 1% FBS, due to strong binding to serum albumin [38].

In addition to the pathway-specific inhibitors some methods for general inhibition of endocytosis was used. The first method was the classic depletion of ATP by 2-deoxyglucose (2-DG) and sodium azide in glucose free media. 2-DG inhibits ATP generation by glycolysis and azide inhibits ATP generation by oxidative phosphorylation [40]. Given the high turn-over of ATP in the cells and the inhibited production, the cells are quickly deprived of ATP and unable to perform most actions, including endocytosis [41]. These experiments were done in glucose free DMEM.

**Efficacy of endocytosis inhibition**

To determine the efficacy of the various methods of inhibiting endocytosis, several control experiments of transferrin endocytosis were performed. Transferrin is endocytosed via CME

and is an ideal compound to investigate the inhibition of CME pathways. Since CME is critically dependent on dynamin, a strong reduction in transferrin endocytosis will serve as a good control for an efficient inhibition of dynamin. The transferrin is marked with radioactive $^{125}I$, which makes it easily detectable using a gamma-counter.

**Experimental procedures**

The HeLaDynK44A cells were seeded out two days prior to experiments in 96-well plates with a density of $3x10^3$ cells/well in 200 µL medium. 48 wells were seeded with tetracycline present (Tet +) and 48 without tetracycline (Tet -). The HeLaDynK44A cell line allowed one extra day before experiments to allow the Tet-Off system to be induced. Drug-loaded PIHCA and empty PIHCA were diluted in medium and added to the cells. Drug concentration in the experiments ranged from 0.1 nM to 10 000 nM of CTX. Concentration of empty nanoparticles ranged from 0.1 µg/ml to 300 µg/ml. The plates were then incubated for the preferred duration, usually 4 hours, but 24 hours was also tried. Three replicates were used for each sample, the control cells had two sets of 3 replicates. The control wells were treated identically to the other wells, with the exception of nanoparticles during the incubation. After the 4 hour incubation, the cells were washed and chased for 48 hours.

For the experiments using inhibitors, MDA-MB-231 was seeded out the day prior to the experiments in 96-well plates with a density of $5x10^3$ cells/well in 200 µL medium. 24 wells were used for each inhibitor and 24 wells without inhibitors. The cells were preincubated 30 minutes with the inhibitors before addition of drug-loaded PIHCA in concentrations ranging from 1 nM to 1000 nM of CTX. The cells were then incubated for 2 hours. The control wells were treated identical to the other wells with the exception of nanoparticles during the incubation. The concentrations used for the inhibitors were 30 µM for Dyngo, 150 µM for CK-666 and 30 µM for Latrunculin B. After the incubation, the cells were washed and chased for 48 or 72 hours.

For the experiments using 2-DG and sodium azide for ATP depletion, HeLaP was seeded out the day prior to the experiments in 96-well plates with a density of $5x10^3$ cells/well in 200 µL medium. 48 wells had medium replaced with depletion media at the same moment as addition of drug-loaded PIHCA in concentrations ranging from 0.3 to 1000 nM of CTX or empty PIHCA in concentrations ranging from 0.3 to 300 µg/ml. The plates were then incubated for 2 or 3 hours. The control wells were treated identical to the other wells with the exception of

nanoparticles during the incubation. The concentration of 2-DG and sodium azide was 6 or 50 mM and 10 mM respectively.

At the day of measurement the cells were measured using either the MTT or the CellTiter-Glo assay.
If the cells were measured using the MTT assay the cells were washed and added 100 µL of 0.25 mg/ml MTT working solution in each well, the plates were then put back in the incubator for 2 hours. After this incubation the MTT solution was removed and the cells were added 100 µL DMSO with 8 mM ammonia to dissolve the formazan crystals.
If the cells were measured using the CellTiter-Glo assay the wells had 100 µL of their medium removed, leaving 100 µL in each well, and equilibrated to room temperature. 100 µL of the CellTiter-Glo reagent was then added to each well and shaken for 10 minutes.

The plates were read in a Synergy 2 (BioTek instruments Inc, USA) plate counter. For the MTT assay the absorbance was measured at 570 nm and 650 nm. 570 is the absorbance value of the formazan. The 650 value is subtracted from the 570 value to eliminate the background absorbance in the wells. For the CellTiter-Glo assay the luminescence was measured. Data from these experiments were processed in Gen5™ (BioTek. Version 1.11) and analyzed in Microsoft Excel 2007/2013.

The control experiments with transferrin were prepared slightly differently for each cell line and type of experiment, however the steps of the experiment is universal. The preparation steps for the different control experiments are as follows:
For controlling the dynamin-inhibition of HeLaDynK44A plates were seeded out simultaneously as the 96-well plates for the toxicity assays. The cells were seeded out two days prior to experiments in 12-well plates with a density of $4x10^4$ cells/well in 1 mL medium. Three wells were seeded with tetracyclin and three without tetracyclin.
For controlling the efficacy of the inhibitors MDA-MB-231 was seeded out the day prior to the experiment in 12-well plates with a density of $4x10^4$ cells/well. The cells were preincubated with the inhibitors in hepes buffered medium for 30 minutes prior to the steps below. Three wells were incubated with each inhibitor and three wells were used for control.
For controlling the endocytosis inhibition achieved by depleting ATP HeLaP was seeded out the day prior to experiments in 12-well plates with a density of $4x10^4$ cells/well. The cells were incubated in depletion media for varying durations prior to the steps below.

The following steps were identical for all transferrin endocytosis experiments:
The cells were washed and the medium was replaced with 300 µL Hepes buffered medium. The cells were then incubated for 30 minutes in an incubator at 37°C. 15 µL of $^{125}$I-Transferrin ($1x10^6$ counts per minute (cpm)) was added to each well and the plates were then incubated for 5 minutes. After the incubation the wells were washed three times with cold dialysis buffer before 300 µL ice cold hepes buffered medium with 2 mg/ml pronase was added to each well. The plates were then incubated on ice for 1 hour. The contents of each well were then transferred to Eppendorf tubes and was centrifuged with a Centrifuge 5417R (Eppendorf AG, Germany) at 4°C, with 14 000 rpm for 5 minutes. The supernatant of each tube was extracted to another Eppendorf tube and the cpm of the pellet and supernatant of each well was counted using a gamma counter, 1261 Multigamma (PerkinElmer Inc, USA). The following formula is used to calculate the relative amount of endocytosed transferrin:

$$Transferrin\ endocytosed\ (\%) = \frac{cpm(Pellet)}{cpm(Total)} \times 100$$

# 3. Results

An initial experiment was performed to find the optimal conditions and a suitable concentration range for the experiments. The range was calculated to be approximately 1-100 nM of cabazitaxel (CTX) or higher than 1-10 µg/ml of the empty nanoparticles. The cells were incubated with drug-loaded or empty nanoparticles for 2 or 4 hour pulse followed by a 48 hour chase.

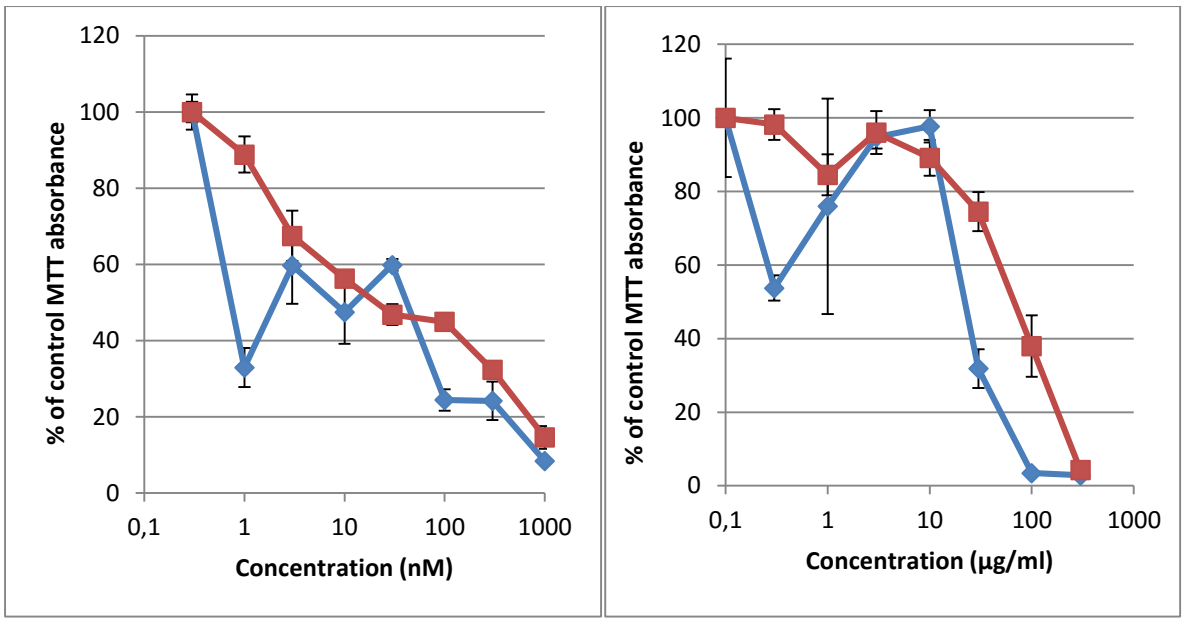


**Figure 3.1. Toxicity of PIHCA loaded with CTX (left) and empty PIHCA (right) in HeLaP after 4 hours (blue) and 2 hours (red) of incubation before removal of nanoparticles, followed by a 48 hour chase.**

This experiments shows a gradual toxicity of both drug and particle, eliminating ~90% of the cells at the highest concentrations. The $IC_{50}$ after 2 hours for the drug-loaded nanoparticles is ~15 nM and 70 µg/ml for the empty nanoparticles.

Another experiment was performed to investigate if the two different batches of nanoparticles (BBB-31 and NC-103) displayed different toxicity as a result of different loading of CTX. The experiment also shows the difference between toxicity after a 4 hour pulse, with a concentration range of 0.1 to 1000 nM of CTX, followed by a 48 hour chase, compared to a continuous 48 hour incubation with a concentration range of 0.01 to 100 nM of CTX.

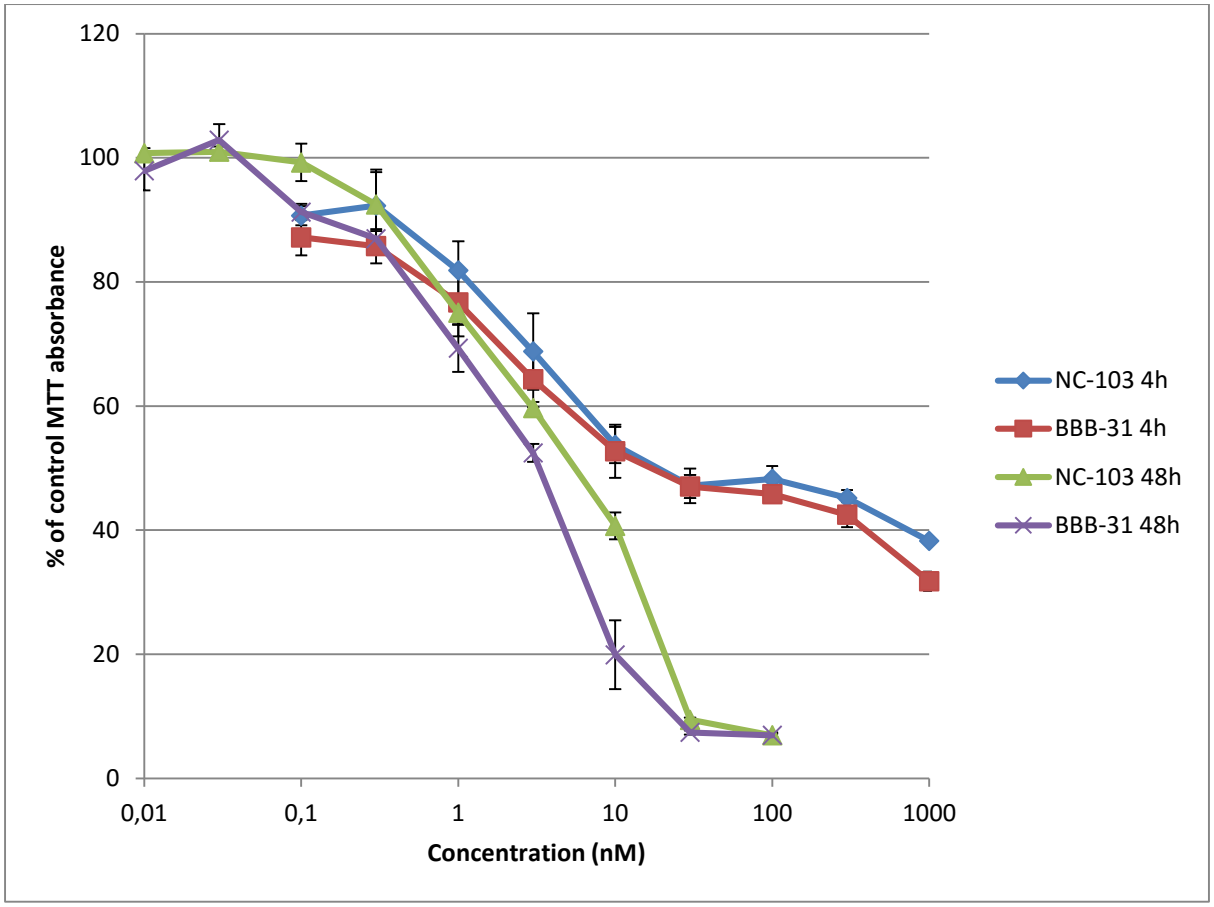


**Figure 2. Toxicity of drug-loaded PIHCA batches BBB-31 after 4 h incubation and 48 h chase (red) or 48 h continuous incubation (purple) and NC-103 after 4 h incubation and 48 h chase (blue) or 48 h continuous incubation (green).**

This experiment shows an $IC_{50}$ after 4 hours incubation of ~15 nM for both batches of nanoparticles. After 48 hours continuous incubation the $IC_{50}$ is 3.5 nM for BBB-31 and 5.5 for NC-103. A similar experiment was performed in the MDA-MB-231 cell line (Appendix figure 1).

## 3.1 Cytotoxicity test in dynamin-deficient cells

In order to address whether uptake of the PIHCA particles loaded with cabazitaxel via dynamin-dependent endocytosis, experiments were performed on the HeLaDynK44A cell line, in cells with tetracycline present (Tet +) and cells deprived of tetracycline (Tet -). In the 'Tet -' condition, dynamin-dependent endocytosis should be inhibited. To ascertain that the dynamin inhibition was sufficient transferrin-endocytosis control experiments were performed routinely throughout these experiments.

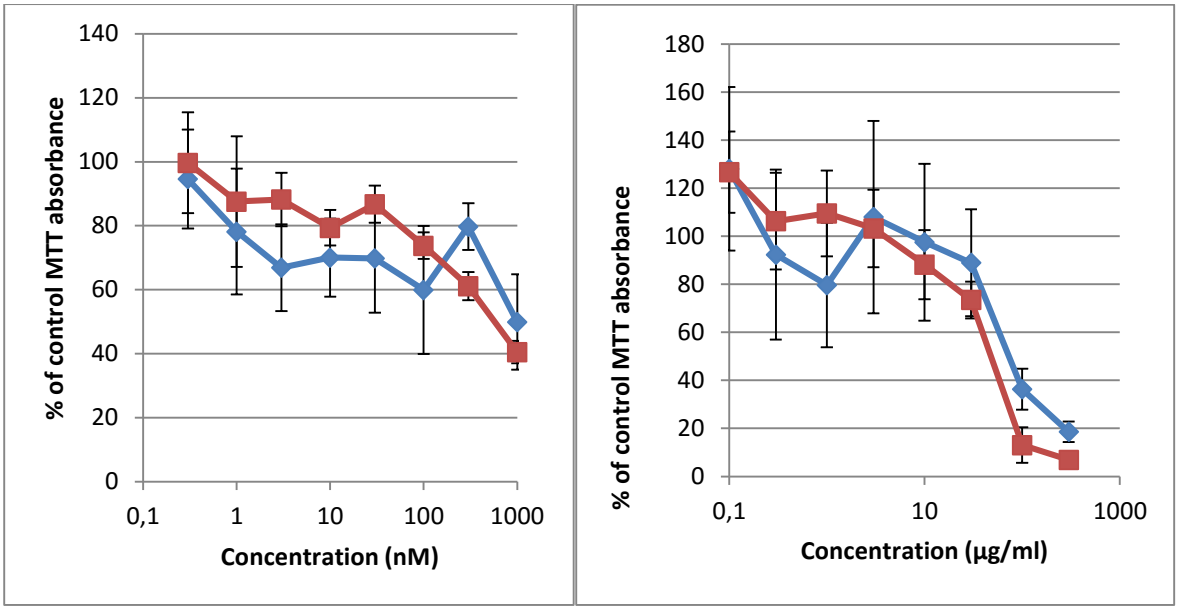


**Figure 3.3. Toxicity of PIHCA loaded with CTX (left) and empty PIHCA (right) in HeLaDynK44A after 4 hours of incubation before removal of nanoparticles in Tet + (red) and Tet - (blue).**

The loaded particles has an $IC_{50}$ for Tet + is 500nM and 1000 nM for Tet -. For the empty particles the $IC_{50}$ for Tet + is ~48µg/ml and ~70 µg/ml for Tet -.

This experiment shows a 1.5 –2 times protection in Tet + compared to Tet -, for both the drug-loaded and empty PIHCA.

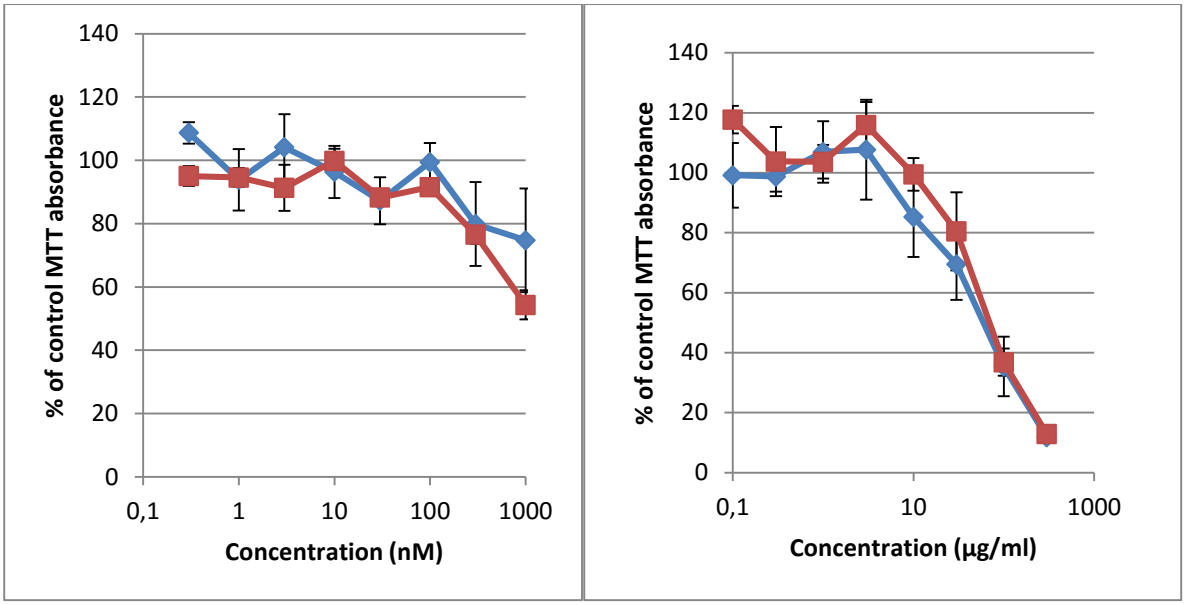


**Figure 3.4. HeLaDynK44A. Toxicity of PIHCA loaded with CTX (left) and empty PIHCA (right) after 4 hours of incubation before removal of nanoparticles in Tet + (red) and Tet - (blue), followed by a 48 hour chase.**

The toxicity of the drug-loaded PIHCA was too low to calculate an $IC_{50}$. The $IC_{50}$ for the empty nanoparticles was 70 µg/ml for Tet + and 60 µg/ml for Tet -.
In this experiment a less than ideal reduction in transferrin endocytosis was observed.

This experiment (Figure 3.4) shows no discernible difference in toxicity in Tet + in comparison to Tet -. The cell line also proved more resistant to cabazitaxel than HeLaP. Both these toxicity experiments show that 40%-50% of the cells remain metabolically active after a 4h pulse at 1000 nM with drug-loaded PIHCA and 48h chase.
Another toxicity experiment and corresponding endocytosis experiment was performed. This time the drug concentration of cabazitaxel was increased to 10 000 nM, for control purposes empty nanoparticles was also used in the experiment. The chase was reduced to 24h. An MTT and CellTiter-Glo assay were done simultaneously, both showing similar results.

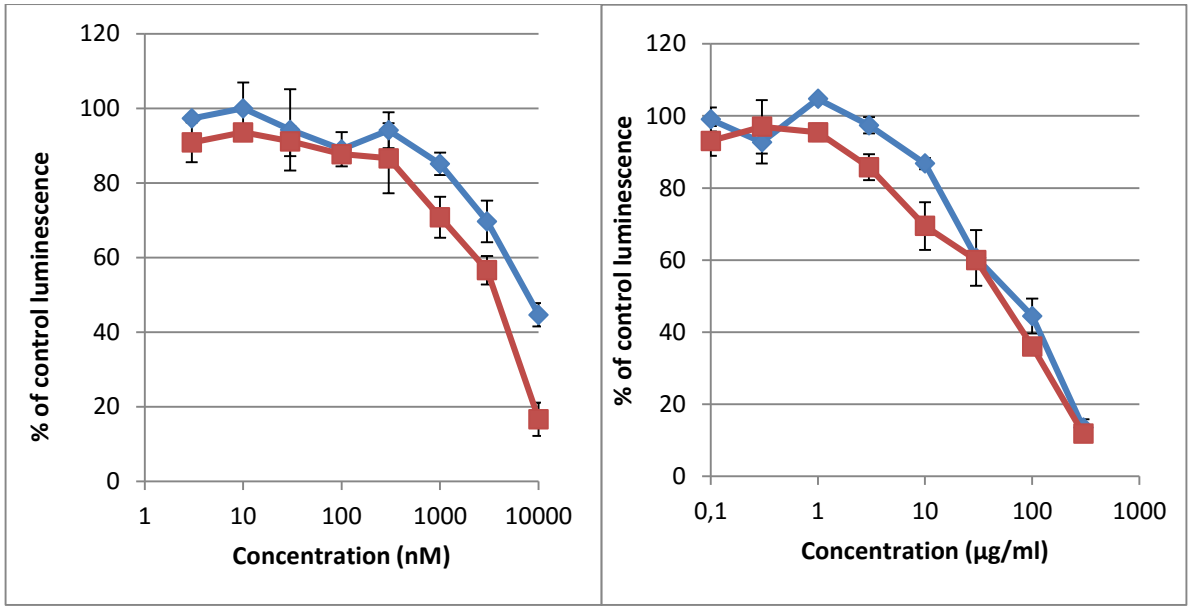


A B

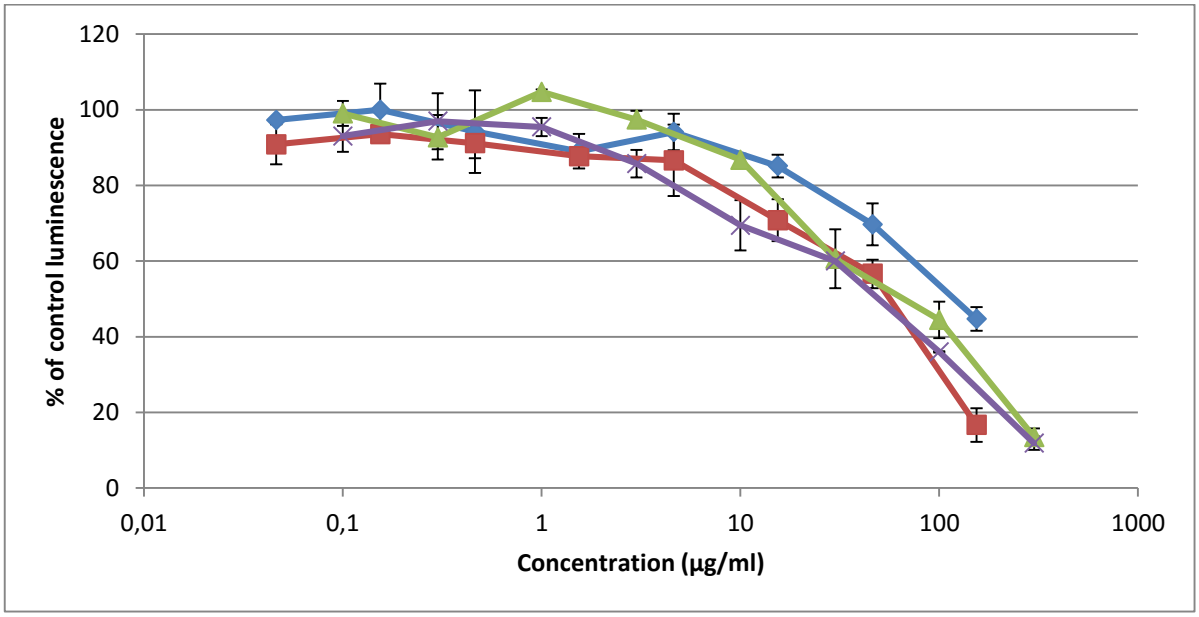


C

**Figure 3.5. Toxicity of PIHCA loaded with CTX (A) and empty PIHCA (B) in HeLaDynK44A cells after 4 hours of incubation with nanoparticles for cells with tetracycline (red) and deprived of tetracycline (blue) followed by a 24 hour chase. C shows a combined graph of A and B with loaded nanoparticles showing toxicity in Tet - (blue) and Tet + (red) and empty nanoparticles in Tet - (green) and Tet + (purple) plotted against their respective concentrations of nanoparticles.**

The $IC_{50}$ of Tet + is 3500 nM, corresponding to a PACA concentration of ~55µg/ml and 8000 nM, corresponding to a PACA concentration of ~120 µg/ml, for Tet -. For the empty nanoparticles there is an $IC_{50}$ of 50 µg/ml for Tet + and 65 µg/ml for Tet -.

The experiment (Figure 3.5.a) shows a doubling of $IC_{50}$ of the loaded nanoparticles in the dynamin impaired cells, which indicates a 2 times protection, but overall there is little or no difference in the toxicity of the cells with normal or impaired function of dynamin, even with a strong reduction in endocytosis (Appendix table 4).

To check if the cell line is truly resistant a control experiment was performed. Free cabazitaxel was used as a control. The plates were incubated continuously for 24 hours.

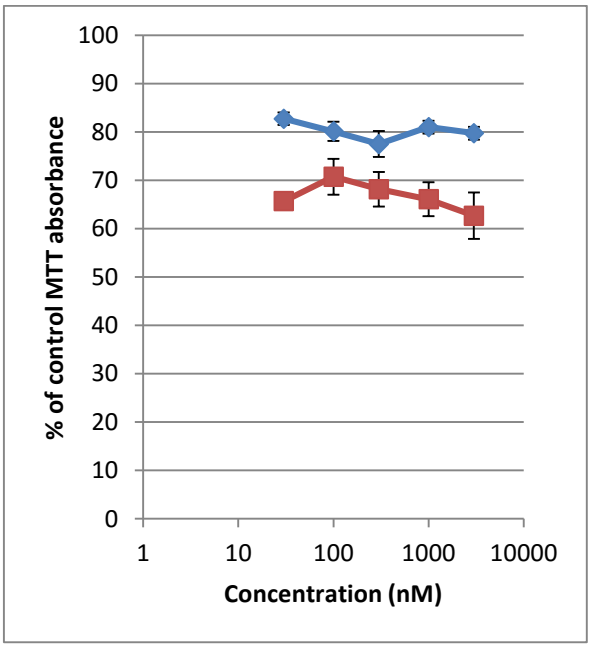


A

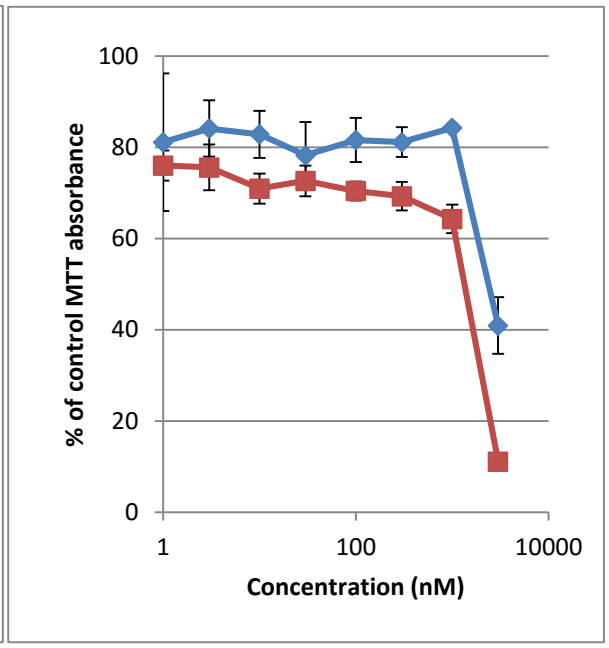


B

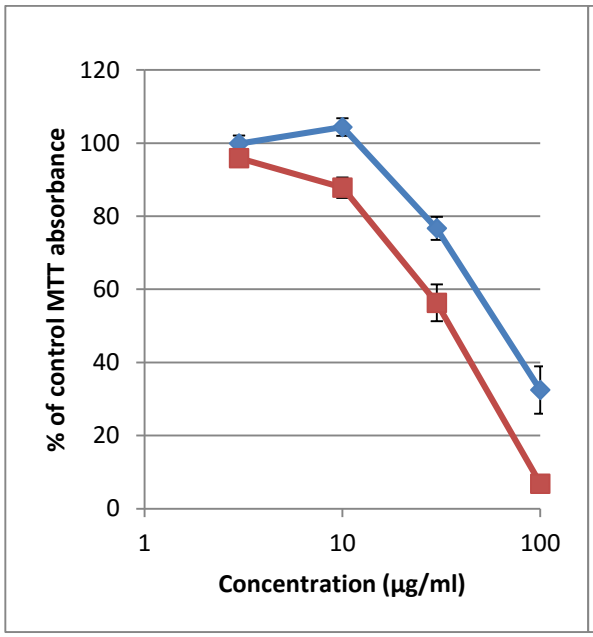


C

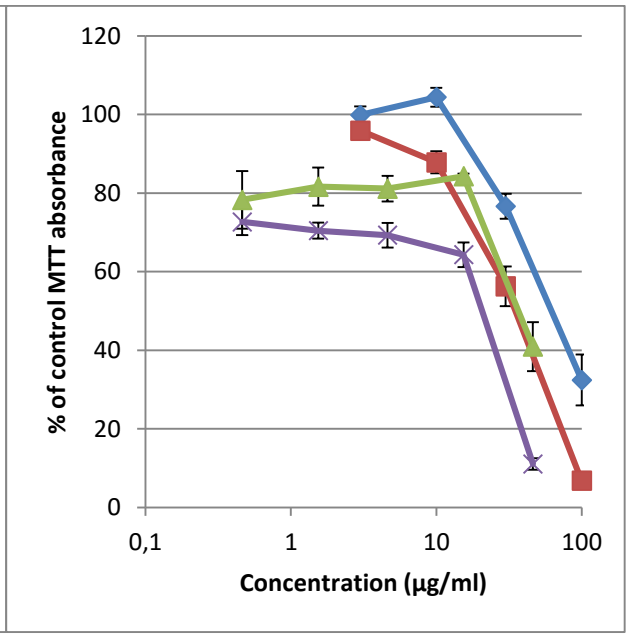


D

**Figure 3.6. Toxicity of CTX (A), PIHCA loaded with CTX (B) and empty PIHCA (C) in Tet - (blue) and Tet + (red) after 24 hours continuous incubation. D is a merge of B and C, with loaded PIHCA in Tet - (green) and Tet + (purple) or empty PIHCA in Tet - (blue) and Tet + (red), plottet for their respective concentrations of nanoparticles.**

There does not seem to be gradual toxicity of the free cabazitaxel (Figure 3.6A), just a flat 20% reduction in cell viability for Tet - and 30-40% reduction in Tet +. This overlaps with the same concentrations of drug encapsulated in nanoparticles (figure 3.6B). The $IC_{50}$ of the loaded nanoparticles are ~1500 nM, corresponding to a PIHCA concentration of ~20 µg/ml, for Tet + and ~2500 nM, corresponding to a PIHCA concentration of 35 µg/ml, for Tet -. The $IC_{50}$ of the empty particles is 35 µg/ml for Tet + and ~60 µg/ml for Tet -. Over a continuous 24 hour incubation there seem to be a slightly more toxic effect of the loaded PIHCA nanoparticles than the empty nanoparticles.

In figure 3.6D a shift can be seen in the relative viability of the cells treated with loaded PIHCA compared to empty PIHCA. However there is no gradual toxicity of the loaded nanoparticles as seen in the HeLaP cells. There seem to be a slight difference between Tet - and Tet +.
A second control experiment was performed to see if another drug, docetaxel, could be used (Appendix figure 2). The experiment showed no toxicity of docetaxel or cabazitaxel.

With this cell line proving resistant to taxanes, other ways to stop endocytosis were tested in HeLaP cells.

## 3.2. Cytotoxicity test in ATP-depleted cells

In a control experiment, sodium azide and 2-deoxy-glucose was tested to ascertain the cell's survivability over various durations (See appendix, figure 3). The results were satisfying and the following experiment was done using 10 mM Na-Azide and 6 mM 2-DG. Half the wells of each plate where depleted with 2-DG and Na-Azide in glucose-free DMEM medium, further mentions of this combination will be referenced as depletion media. Depletion media and nanoparticles were added simultaneously. The cells were incubated with nanoparticles for 3 hours and chased for 48 hours.

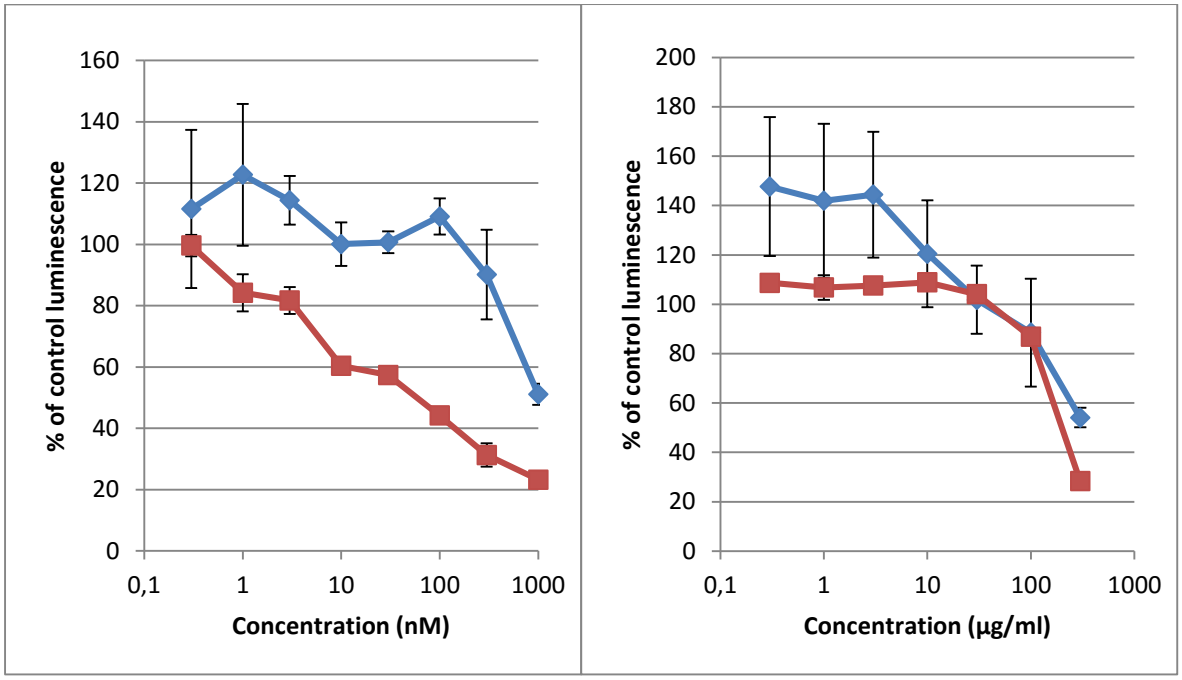


**Figure 3.7. Toxicity of PIHCA loaded with cabazitaxel (left) and empty PIHCA (right) in HeLaP after 3 hours of incubation before removal of nanoparticles for cells depleted of ATP with 10 mM Na-Azide and 6 mM 2-DG (blue) and untreated (red), followed by a 48 hour chase.**

This experiment shows a definite shift in toxicity of drug-loaded PIHCA in depleted cells compared to controls. The $IC_{50}$ of loaded particles was 60 nM, corresponding to 0.9 µg/ml, for the control cells and 1000 nM, which corresponds to 15 µg/ml, for the depleted cells. The empty nanoparticles showed an $IC_{50}$ of 200 µg/ml in the control cells. The experiment was repeated two times with similar results.

For the next experiments the concentration of 2-DG was increased to 50 mM and the incubation time with nanoparticles reduced to 2 hours.

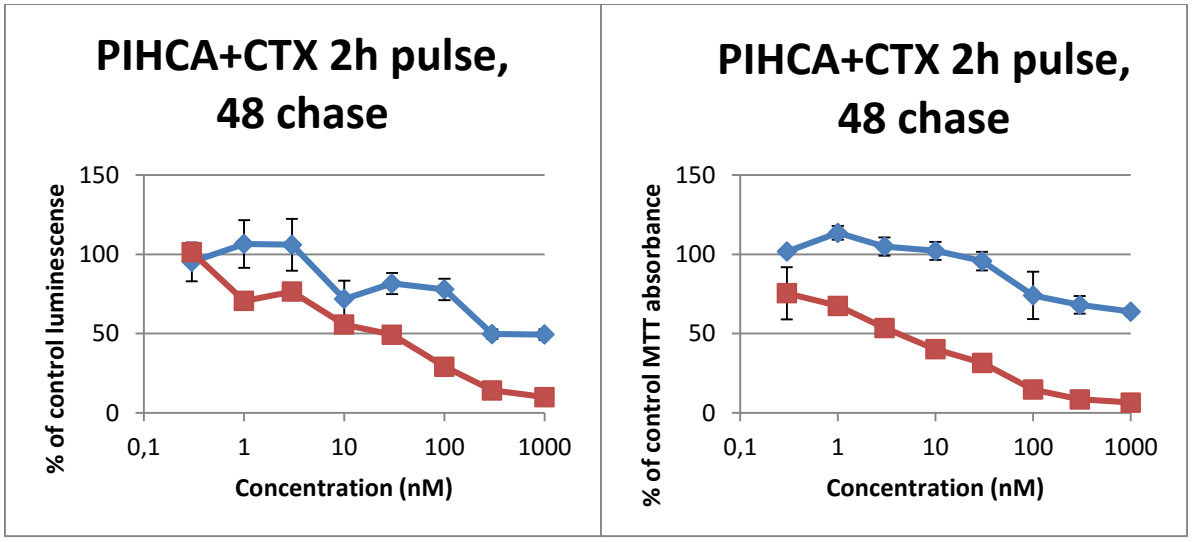


A B

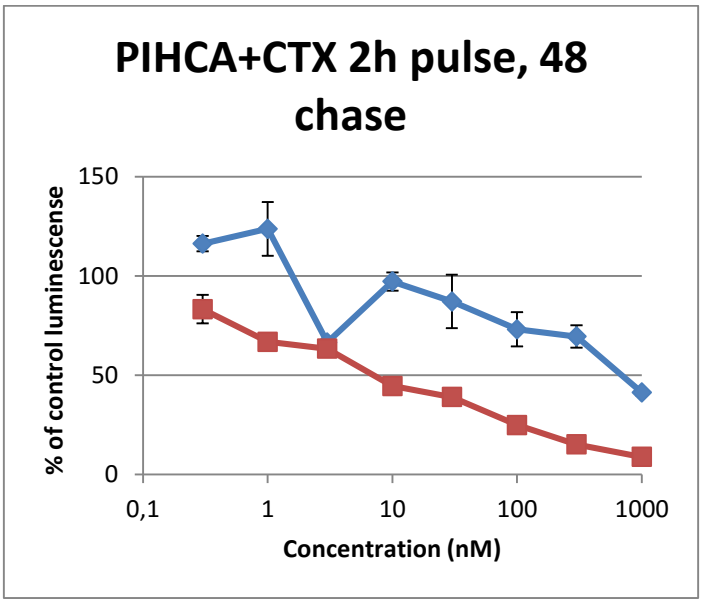


C

**Figur 3.8. Toxicity of PIHCA loaded with CTX in HeLaP after 2 hours of incubation with nanoparticles in cells depleted of ATP with 50 mM 2-DG 10 mM Na-Azide (blue) and untreated (red).**

Three experiments were performed with concentrations of PIHCA+CTX ranging from 0.3 to 1000 nM concentrations of CTX. Half the cells were treated with depletion media during incubation with nanoparticles. The experiment shown in figure 3.8A shows an $IC_{50}$ of 30 nM, which corresponds to 0.4 µg/ml concentration nanoparticles, for the control cells and 300 nM, corresponding to 4.5 µg/ml concentration of nanoparticles, for the depleted cells. The second experiment (figure 3.8B) shows an $IC_{50}$ of 4 nM in the control cells, while the last experiment (figure 3.8C) shows an $IC_{50}$ of 7 nM, corresponding to ~0.1 µg/ml, for the control cells and 700 nM, corresponding to ~10 µg/ml for the depleted cells.

The experiment shows a clear difference in toxicity in the cells depleted of ATP compared to the control cells.

## 3.3 Inhibition of clathrin-mediated and actin-dependent endocytosis.

To investigate the effect of endocytosis further, a series of experiments were performed where the cells were treated with three different inhibitors. These experiments were done in the MDA-MB-231 cell line.

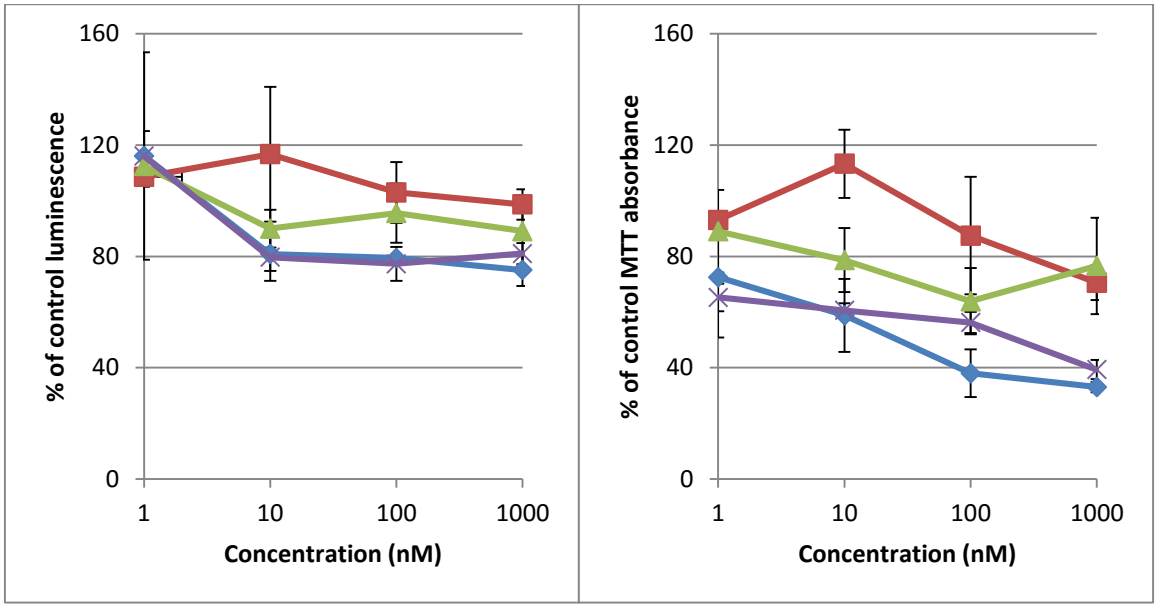


**Figur 3.9. Toxicity of PIHCA loaded with CTX in MDA-MB-231. Cells were preincubated 30 minutes with inhibitors CK-666 (purple), dyngo (green) and latrunculin B (red) or without inhibitors (blue) before incubation with PIHCA+CTX for 2 hours, followed by a 48 hour chase.**

Five experiments were performed with concentrations of loaded PIHCA ranging from 1 to 1000 nM of cabazitaxel. The cells were preincubated with inhibitors for 30 minutes, followed by a 2 hour pulse with nanoparticles before nanoparticles and inhibitors were removed. The cells were washed followed by a subsequent 48 hour chase. Four of the experiments showed similar results.

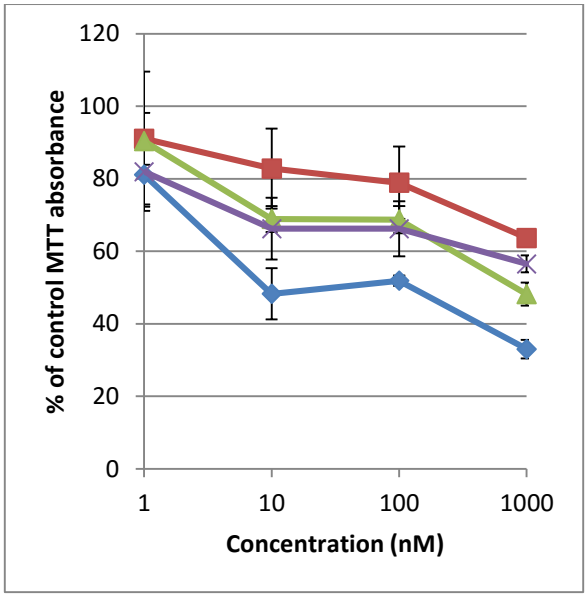


**Figure 3.10. Toxicity of PIHCA loaded with CTX in MDA-MB-231. Cells were preincubated 30 minutes with inhibitors CK-666 (purple), dyngo (green) and latrunculin B (red) or without inhibitors (blue) before incubation with PIHCA+CTX for 2 hours, followed by a 72 hour chase.**

Four experiments were performed with concentrations of loaded PIHCA ranging from 1 to 1000 nM of cabazitaxel. The cells were preincubated with inhibitors for 30 minutes, followed by a 2 hour pulse with nanoparticles before nanoparticles and inhibitors were removed. The cells were washed followed by a subsequent 72 hour chase.

## 3.4 Microscopy studies

**Endocytosis and uptake of nanoparticles containing NR668**

Colocalization studies between LAMP-1 and drug-loaded PIHCA containing NR668 were performed, however in the relevant concentration range of encapsulated CTX the concentration of nanoparticles proved too small to properly analyse. A few cells showed some uptake, but it was difficult to determine if the particles were colocalized with the lysosomes (data not shown).

**Mechanism of cell death of encapsulated cabazitaxel**

HeLaP cells were incubated with concentration ranges of 1 to 1000 nM of CTX encapsulated in PIHCA for 4 hours followed by a 24 or 48 hour chase. The cells were stained with antibody against cleaved PARP (green) and DAPI (blue), the contrast image is also included to show the borders of the cells.

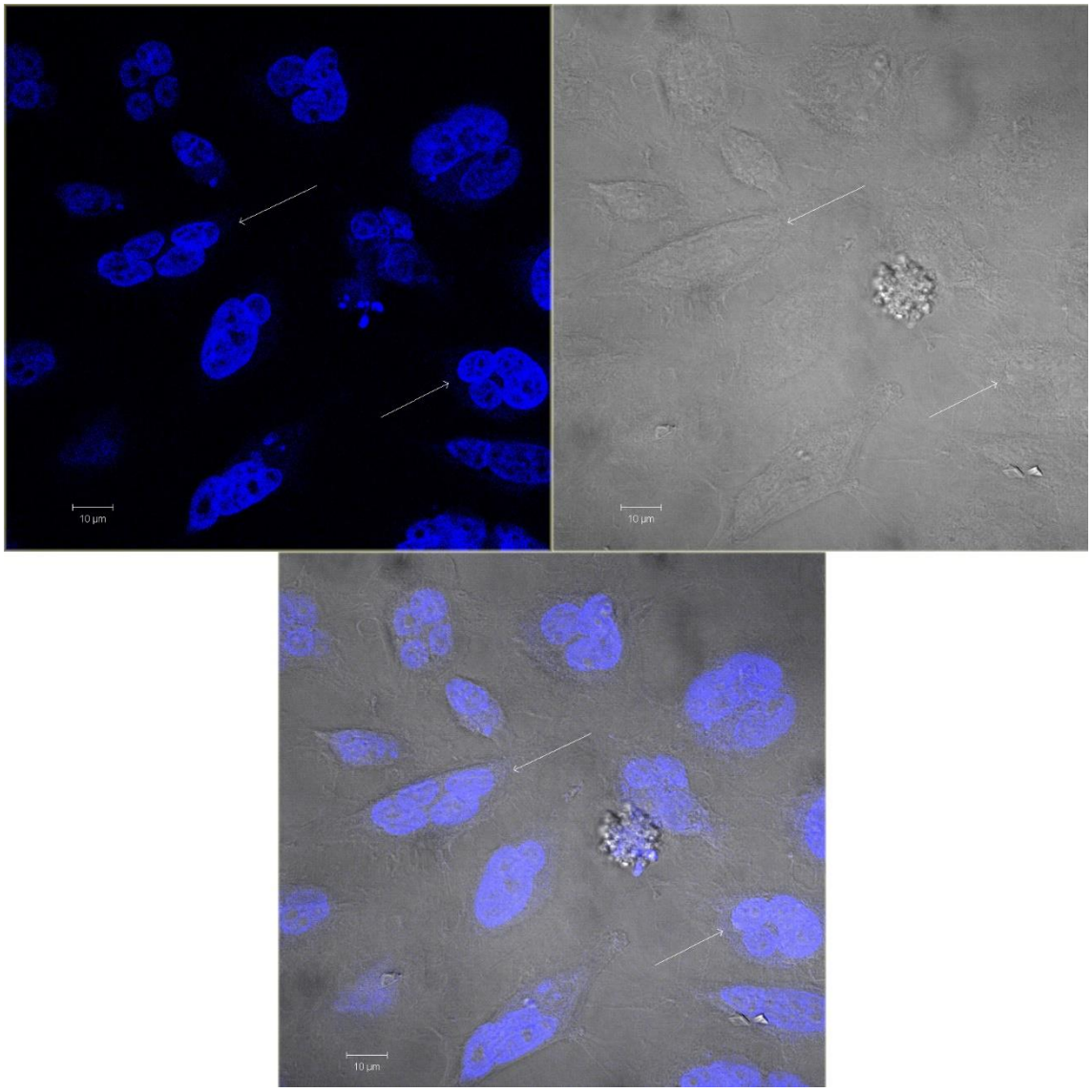


**Figure 3.11. Confocal fluorescence image of cell death induced after 4 hours incubation with 1nM PIHCA loaded with CTX, followed by a 24 hour chase.**

A representative figure of one of the covers slips incubated with 1 nM and chased for 24 hours is shown in figure 3.11 and 3.12. In figure 3.11 the green channel is removed. Figure 3.11 shows two or more tetraploid multinuclear cells (marked with arrows). At 10 and 100 nM more cleaved PARP positive cells were observed. At 1000 nM, however, fewer apoptotic and more multinuclear cells were observed.

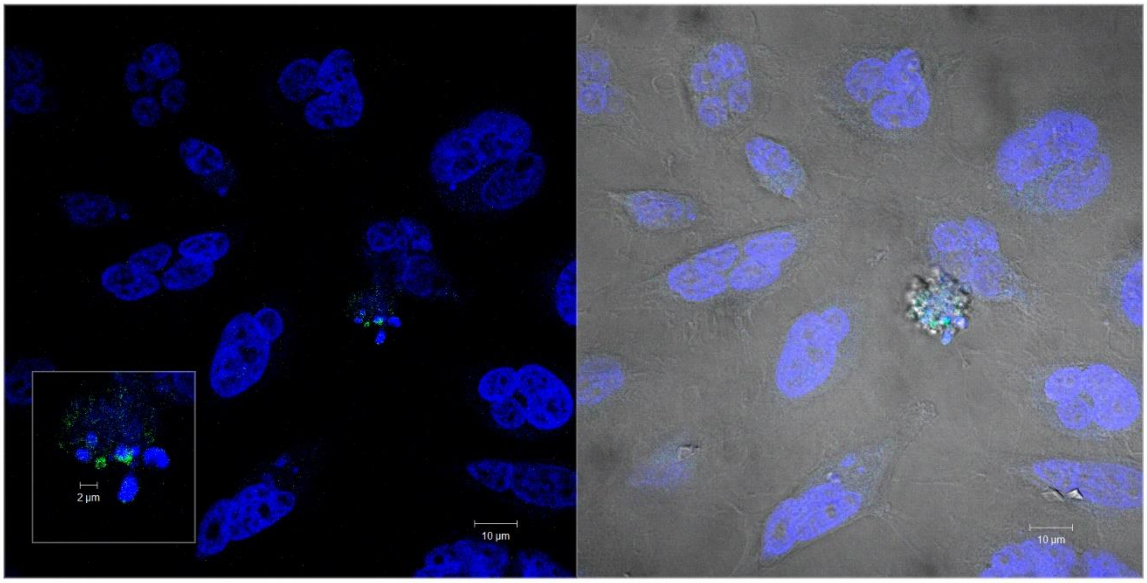


**Figure 3.12. Confocal fluorescence image of cell death induced after 4 hours incubation with 1nM PIHCA loaded with CTX, followed by a 24 hour chase. With 2 µm inset (left) and contrast (right)**

Figure 3.12 shows the same image but with the channel showing cleaved PARP in the apoptotic cell, the inset shows a 5 times zoom of the apoptotic cell without contrast.

# 4. Discussion

The toxicity of the nanoparticles on HeLaP cells (figure 3.1) shows expected level of toxicity for both the drug-loaded and the empty nanoparticles. The graph in figure 3.2 shows shows that a 4h pulse is sufficient to elicit a toxic effect. An interesting phenomenon is shown in this figure, the difference toxicity with a 4 hour pulse compared to the continuous 48 hour incubation seem to increase at higher drug concentrations. The toxicity of the drug-loaded particles seem to level off around 50%, at concentrations of 30 – 300 nM. A possible explanation might be that PIHCA uptake reaches a saturation point at approximately 10 nM.

## 4.1 Cytotoxicity test in dynamin-deficient cells.

When starting with the experiments on HeLaDynK44A the inhibition of dynamin was tested to give a ~60% reduction in transferrin endocytosis (Appendix table 1). A maximal dynamin inhibition of over 90% have been observed, however >60% reduction should be sufficient to see an effect.
Figure 3.2 shows that the HeLaDynK44A cell line is far less susceptible to the taxane cytotoxicity, but the toxicity of the empty particles is similar to HeLaP.

Even though the control experiments show an average reduction of endocytosis by ~66% the results shows little difference in toxicity of either the drug-loaded or empty nanoparticles. The transferrin endocytosis experiments showed varying reduction in endocytosis. This could be a result of traces of tetracyclin remaining in the cells, *however* confluent cells with reduced protein synthesis will also have a slower synthesis of the dominant negative dynamin. These factors can contribute to the poor inhibition of dynamin in the cells.
The low toxicity of the loaded particles prompted an increase in concentration to 10 000 nM, which corresponds to ~150 µg/ml of nanoparticles. The toxicity seen at this concentration is likely due to toxicity of the nanoparticles themselves (Figure 3.4).
To be certain of the HeLaDynK44A cell lines resistance to taxanes a control experiment was performed, with free cabazitaxel, drug-loaded and empty PIHCA being incubated continuously

for 24 hours with the cells (Figure 3.6). The graph of both free cabazitaxel and loaded PIHCA starts at about 80% for 30 nM and 1 nM respectively. This, and the shift seen in 3.6.A and B between Tet - and Tet + could be caused by a problem during the seeding of the cells. Cell count for Tet + in this experiment was consistently 60% lower than Tet -, even in the control wells (data not shown). The experiments in figure 3.2 and 3.6 show a 2-fold protection in the Tet - cells with the dominant negative dynamin, this effect was more pronounced in the experiments where the cells were continuously incubated for 24 hours compared to the experiments were incubated for 4 hours and washed off. This is likely due to the noticeable increase in toxicity at high concentrations of nanoparticles.

Another experiment with free cabazitaxel was performed because of the unreliability of the last experiment. In this experiment docetaxel was also added as a secondary control. This experiment (Appendix figure 2) showed no toxicity of either cabazitaxel or docetaxel. This experiment didn't show any difference in toxicity of the nanoparticles in Tet + compared to Tet - (Appendix figure 2C). It is unknown why this cell line has proven resistant to taxanes. One possible explanation is that the cell line has developed multidrug resistance (MDR). There are several possible mechanisms for MDR, famously P-gp, an ATP-driven efflux pump. However this is an unlikely explanation considering cabazitaxels low affinity for the P-gp pump compared to other taxanes [31]. Other mechanisms of MDR have been reported and a possible candidate is mutation induced alterations in tubulin expression or alterations in the physical properties of microtubules [42].

## 4.2 Cytotoxicity test in ATP-depleted cells

The control experiment (Appendix figure 3) shows a strong depletion after 2 hours. According to previous data with HeLaP the optimal incubation time was 4 hours to ensure endocytosis of the nanoparticles, however the control experiment showed a >50% reduction of viable cells after a 4 hour depletion. A transferrin endocytosis experiment was performed to see the reduction of endocytosis at different time points after starting depletion (Appendix table 8). Based on these two control experiments the cells were incubated with nanoparticles for 3 hours. 3 hours showed less reduction in cell viability and showed a satisfying reduction of endocytosis compared to 4 hours.

The treatment shows a clear protection from the toxicity of the loaded nanoparticles (figure 3.7). The treatment provided the cells an average 10-fold increased protection against the

toxicity of the drug-loaded nanoparticles, this indicates that endocytosis is important for the toxicity of drug-loaded PIHCA. The depleted cells did not show significant protection from the toxicity of the empty particles in any of the experiments. This suggests that the toxicity of the nanoparticles is not dependent on endocytosis to elicit a toxic effect.

A control experiment was performed to see if it was possible to increase the efficiency of depletion in a way that would reduce the incubation time needed, in order to reduce standard deviations (Appendix table 6). The three experiments in figure 3.8 shows varying degrees of protection, but all show a very strong protection in the depleted cells. The protection yielded in these experiments ranged from 10-fold to 100-fold increased protection against the drug-loaded PIHCA particles.

## 4.3 Inhibition of clathrin-mediated and actin-dependent endocytosis

The first experiments with inhibitors (3.9) showed a clear protection in the cells treated with dyngo and latrunculin B. This suggests that dynamin and actin are important in the pathways used to endocytose the PIHCA particles. The MDA-MB-231 cell line is multidrug resistant and thus vastly less susceptible to taxane toxicity than the HeLaP cell line. Studies have shown that this cell line can induce autophagy to avoid toxicity induced by taxanes [Notte, Ninane]. This could be one explanation for why this cell line is more resistant to cabazitaxel.

In an attempt to overcome this mechanism, the chase was increased to 72 hours. These experiments (figure 3.10) showed greater toxicity than the experiments shown in figure 3.9, though not as effective as in HeLaP. One experiment showed no significant protection by latrunculin B and indeed showed greater toxicity in the cells incubated with CK-666 than with PIHCA+CTX alone. In three of the experiments however, the results were similar to the results shown in figure 3.10, with all three inhibitors showing a clear protection against the toxicity of the drug-loaded PIHCA. Overall, latrunculin B showed greater protection than the other inhibitors, suggesting that actin-dependent mechanisms are dominating in endocytosis of PIHCA nanoparticles.

## 4.4 Microscopy studies

Even after a 24 hour chase at 1 nM some apoptotic bodies could be seen, however the incidence was low. About 1 in 20 cells were apoptotic at this concentration and time and 1-2 in 20 were multinucleated. At 10 nM the amount of apoptotic cells increased to 2 in 20 and 3 in 20 for multinucleated cells. At 100 and 1000 nM at 48 hours there were fewer apoptotic cells than at lower concentrations. At these concentrations however, there was a higher number of multinucleated cells, approximately 5 in 20 at 100 nM and 8-9 in 20 at 1000 nM. The reason could be that at this concentration most of the cells and the apoptotic cells in particular, had already fallen off the cover slip before fixation.

Figure 3.11 shows a few multinucleated cells. This happens due to mitotic slippage during the mitotis stage of the cell cycle. The cells produce a secondary set of DNA, but cannot divide, resulting in two nuclei, if this happens again the cell will have four nuclei, as seen in the figure. After a cell endures this process, they often go into apoptosis. Figure 3.12 highlights an apoptotic cell. The right image shows the characteristic blebs accompanying apoptosis. The inset in the left image gives a better view of the cell, it seems like the nucleus is fragmented and is inside apoptotic bodies.

## 4.5 Considerations for further studies

In light of the results of this thesis I have the following suggestions for further studies.

The results of inhibitor experiments (3.9 and 3.10) suggests that actin-dependent endocytosis mechanisms are important in endocytosis of PIHCA. To investigate the actin-dependent pathways I recommend:

- Further studies using amiloride to study uptake of PIHCA through macropinocytosis.
- Further studies to investigate whether or not the RhoA/Rac1 mechanism of the CIE pathway is involved in endocytosis of PIHCA.

The results of the microscopy studies supports earlier observations that taxanes induce apoptosis and multinucleation, but did not conclude anything regarding uptake of the particles loaded with fluorescent dye. To investigate the uptake of nanoparticles in relation to cytotoxicity I recommend

- Live cell imaging of cells to follow the cell from addition of nanoparticles until death to see if apoptosis is the only mechanism involved.

# 5. Conclusion

In this thesis the effect of endocytosis on the toxicity of drug-loaded nanoparticles has been investigated. The dynamin-specific inhibition in the HeLaDynK44A cell line proved inapplicable due to resistance to taxane drugs.

The experiments where ATP-depletion was deployed showed a markedly increase in protection against the drug-loaded PIHCA, but did not seem to cause any difference in the toxicity of the empty nanoparticles. This suggests that the toxicity of the empty PIHCA is not dependent on endocytosis, while the drug-loaded PIHCA are highly dependent on endocytosis to elicit the desired toxic drug response.

The experiments using various inhibitors of endocytic mechanisms corroborates the results of the ATP-depletion experiments. The cells were definitely protected from the toxicity of the drug-loaded PIHCA while under the effects of the inhibitors. The most effective protection was observed when the cells were treated with latrunculin B, suggesting that actin plays an important role in the endocytosis of these nanoparticles in HeLaP cells.

The microscopy study of taxane induced cell death showed that with increasing concentrations there was an increase in the number of multinucleated cells. At concentrations of 100 nM and higher there was a reduction in the number of cleaved PARP positive cells, likely because the apoptotic cells had fallen off the cover slip before fixation.

# 6. References


1. Thorley, A.J. and T.D. Tetley, *New perspectives in nanomedicine.* Pharmacology & Therapeutics, 2013. **140**: p. 176-185.
2. Skotland, T., T.-G. Iversen, and K. Sandvig, *New metal-based nanoparticles for intravenous use: requirements for clinical success with focus on medical imaging.* Nanomedicine: Nanotechnology, Biology and Medicine, 2010. **6**: p. 730-737.
3. Martis, E.A., R.R. Badve, and M.D. Degwekar, *Nanotechnology based devices and applications in medicine: An overview.* Chronicles of Young Scientists, 2012. **3**(1): p. 68-73.
4. Chiellini, F., et al., *Micro/nanostructured polymeric systems for biomedical and pharmaceutical applications.* Nanomedicine, 2008. **3**(3): p. 367-393.
5. Davis, M.E., Z.G. Chen, and D.M. Shin, *Nanoparticle therapeutics: an emerging treatment modality for cancer.* Nature Reviews: Drug Discovery, 2008. **7**: p. 771-782.
6. Aggarwal, P., et al., *Nanoparticle interaction with plasma proteins as it relates to particle biodistribution, biocompatibility and therapeutic efficacy.* Advanced Drug Delivery Reviews, 2009. **61**(6): p. 428-437.
7. Iyer, A.K., et al., *Exploiting the enhanced permeability and retention effect for tumor targeting.* Drug Discovery Today, 2006. **11**(17/18): p. 812-818.
8. Sharma, A., S.V. Madhunapantula, and G.P. Robertson, *Toxicological considerations when creating nanoparticle-based drugs and drug delivery systems.* Expert Opinion on Drug Metabolism & Toxicology, 2012. **8**(1): p. 47-69.
9. Kim, B.Y.S., J.T. Rutka, and W.C.W. Chan, *Nanomedicine.* New England Journal of Medicine, 2010. **363**(25): p. 2434-2443.
10. Ernsting, M.J., et al., *Factors controlling the pharmacokinetics, biodistribution and intratumoral penetration of nanoparticles.* Journal of Controlled Release, 2013. **172**(3): p. 782-794.
11. Nazir, S., et al., *Nanomaterials in combating cancer: Therapeutic applications and developments.* Nanomedicine: Nanotechnology, Biology and Medicine, 2014. **10**: p. 19-34.
12. Griffiths, G., et al., *Nanobead-based interventions for the treatment and prevention of tuberculosis.* Nature Reviews: Microbiology, 2010. **8**: p. 827-834.

13. Vauthier, C., et al., *Poly(alkylcyanoacrylates) as biodegradable materials for biomedical applications.* Advanced Drug Delivery Reviews, 2003. **55**: p. 519-548.
14. Rao, J.P. and K.E. Geckeler, *Polymer nanoparticles: Preparation techniques and size-control parameters.* Progress in Polymer Science, 2011. **36**: p. 887-913.
15. Duncan, R. and S.C.W. Richardson, *Endocytosis and Intracellular Trafficking as Gateways for Nanomedicine Delivery: Opportunities and Challenges.* Molecular Pharmaceutics, 2012. **9**(9): p. 2380-2402.
16. Iversen, T.-G., T. Skotland, and K. Sandvig, *Endocytosis and intracellular transport of nanoparticles: Present knowledge and need for future studies.* Nano Today, 2011. **6**: p. 176-185.
17. McMahon, H.T. and E. Bourcrot, *Molecular mechanisms and physiological functions of clathrin mediated endocytosis.* Nature Reviews: Molecular Cell Biology, 2011. **12**: p. 517-533.
18. Grassart, A., et al., *Pak1 Phosphorylation Enhances Cortactin-N-WASP Interaction in Clathrin-Caveolin-Independent Endocytosis.* Traffic, 2010. **11**: p. 1079-1091.
19. Sandvig, K., et al., *Clathrin-independent endocytosis: mechanisms and function.* Current Opinion in Cell Biology, 2011. **23**: p. 413-420.
20. Khalil, I.A., et al., *Uptake Pathways and Subsequent Intracellular Trafficking in Nonviral Gene Delivery.* Pharmacological Reviews, 2006. **58**(1): p. 32-45.
21. Mellman, I., *Endocytosis and Molecular Sorting.* Annual Review of Cell and Developmental Biology, 1996. **12**: p. 575-625.
22. Gruenberg, J. and H. Stenmark, *The biogenesis of multivesicular endosomes.* Nature Reviews: Molecular Cell Biology, 2004. **5**: p. 317-323.
23. Lherm, C., et al., *Alkylcyanoacrylate drug carriers: II. Cytotoxicity of cyanoacrylate nanoparticles with different alkyl chain length.* International Journal of Pharmaceutics, 1992. **84**: p. 13-22.
24. Alberts, B., et al., *Molecular Biology of the Cell*. 4 ed. 2002, New York: Garland Science.
25. Wani, M.C., et al., *Plant antitumor agents. VI. Isolation and structure of taxol, a novel antileukemic and antitumor agent from Taxus brevifolia.* Journal of the American Chemical Society, 1971. **93**(9): p. 2325-2327.
26. Richard Pazdur, D.o.O.D.P., FDA. *FDA Approval for Docetaxel*. [Web] 28.03.2014 20.05.2016]; Available from: http://www.cancer.gov/about-cancer/treatment/drugs/fda-docetaxel.

27. Jordan, M.A., *Mechanism of Action of Antitumor Drugs that Interact with Microtubules and Tubulin.* Current Medicinal Chemistry - Anti Cancer Agents, 2002. **2**: p. 1-17.
28. Lodish, H., et al., *Molecular Cell Biology*. 4 ed. 2000, New York: W. H. Freeman and Company.
29. Jelínek, M., et al., *The role of individual caspases in cell death induction by taxanes in breast cancer cells.* Cancer Cell International, 2015. **15**: p. 8-23.
30. Abidi, A., *Cabazitaxel: A novel taxane for metastatic castration-resistant prostate cancer - Current implications and future prospects.* Journal of Pharmacology and Pharmacotherapeutics, 2013. **4**(4): p. 230-237.
31. Nightingale, G. and J. Ryu, *Cabazitaxel (Jevtana): A Novel Agent for Metastatic Castration-Resistant Prostate Cancer.* Pharmacy and Therapeutics, 2012. **37**(8): p. 440-448.
32. Riss, T.L., R.A. Moravec, and A.L. Niles, *Cytotoxicity Testing: Measuring Viable Cells, Dead Cells, and Detecting Mechanism of Cell Death*, in *Mammalian Cell Viability*, M.J. Stoddart, Editor. 2011, Humana Press. p. 103-114.
33. Meerloo, J.v., G.J.L. Kaspers, and J. Cloos, *Cell Sensitivity Assays: The MTT Assay*, in *Cancer Cell Culture: Methods and Protocols*, I.A. Cree, Editor. 2011, Humana Press. p. 237-245.
34. Promega. *CellTiter-Glo Luminescent Cell Viability Assay*. 2015; 15].
35. Bucher, D., *A practical guide for fluorescent confocal microscopy*. Marder Labs: brandeis.edu.
36. Klymchenko, A.S., et al., *Highly lipophilic fluorescent dyes in nano-emulsions: towards bright non-leaking nano-droplets.* RSC Advances, 2012. **2**: p. 11876-11886.
37. Genoway. *TET System: Controlled Gene Expression*. 25.04.2016]; Available from: https://www.genoway.com/technologies/tet-system.htm.
38. McCluskey, A., et al., *Building a Better Dynasore: The Dyngo Compounds Potently Inhibit Dynamin and Endocytosis.* Traffick, 2013. **15**: p. 1272-1289.
39. Basquin, C., et al., *Membrane protrusion powers clathrin-independent endocytosis of interleukin-2 receptor.* The EMBO Journal, 2015. **34**(16): p. 2147-2161.
40. Schwoebel, E.D., T.H. Ho, and M.S. Moore, *The mechanism of inhibition of Ran-dependent nulcear transport by cellular ATP depletion.* The Journal of Cell Biology, 2002. **157**(6): p. 963-974.

41. Schmid, S.L. and L.L. Carter, *ATP is Required for Receptor-mediated Endocytosis in Intact Cells.* The Journal of Cell Biology, 1990. **111**(6): p. 2307-2318.
42. Fojo, A. and M. Menefee, *Microtubule Targeting Agents: Basic Mechanisms of Multidrug Resistance (MDR).* Seminars in Oncology, 2005. **32**(Supplement 7): p. 3-8.
43. Bradley, G., P.F. Juranka, and V. Ling, *Mechanism of multidrug resistance.* Biochimica et Biophysica Acta, 1988. **948**: p. 87-128.

# Appendix

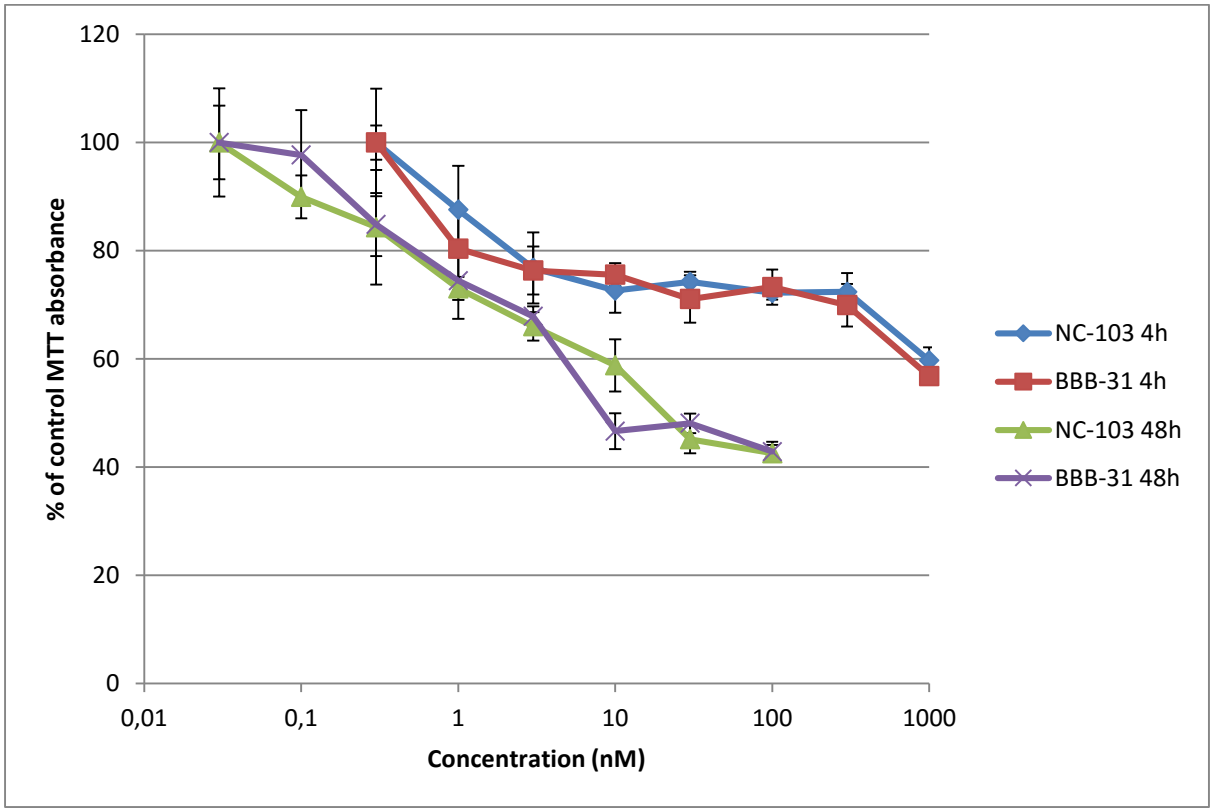


**Appendix Figure 5. Toxicity of drug-loaded PIHCA batches BBB-31 after 4 h incubation and 48 h chase (red) or 48 h continuous incubation (purple) and NC-103 after 4 h incubation and 48 h chase (blue) or 48 h continuous incubation (green).**

**Appendix table 1. Efficacy of dynamin inhibition.**

| Wells | Pellet (cpm) | Supernatant (cpm) | Total (cpm) | % endocytosed | Reduction of endocytosis % |
|---|---|---|---|---|---|
| **Tet +** | 16 219.3 | 22 441.9 | 38 661.2 | 42% | |
| **Tet -** | 12 160.2 | 65 603.6 | 77 763.8 | 15.6% | 62.7% |

**Appendix table 2. Efficacy of dynamin inhibition.**

| Wells | Pellet (cpm) | Supernatant (cpm) | Total (cpm) | % endocytosed | Reduction of endocytosis % |
|---|---|---|---|---|---|
| **Tet +** | 1 944.1 | 3 766.8 | 5 710.8 | 34% | |
| **Tet -** | 1 176.5 | 12 199.8 | 14 376.3 | 8.2% | 76% |

**Appendix table 3. Efficacy of dynamin inhibition.**

| Wells | Pellet (cpm) | Supernatant (cpm) | Total (cpm) | % endocytosed | Reduction of endocytosis % |
|---|---|---|---|---|---|
| **Tet +** | 14 075.8 | 14 643.4 | 28 719.2 | 49% | |
| **Tet -** | 7 522.9 | 24 332.2 | 31 855.1 | 23.6% | 51.8% |

**Appendix table 4. Efficacy of dynamin inhibition.**

| Well | Pellet (cpm) | Supernatant (cpm) | Total (cpm) | % endocytosed | Reduction of endocytosis % |
|---|---|---|---|---|---|
| **Tet +** | 816.2 | 2 838.7 | 3 654.9 | 22.3% | |
| **Tet -** | 516.4 | 9 764.2 | 10 280.6 | 5% | 77.5% |

**Appendix table 5. Efficacy of dynamin inhibition.**

| Well | Pellet (cpm) | Supernatant (cpm) | Total (cpm) | % endocytosed | Reduction of endocytosis % |
|---|---|---|---|---|---|
| **Tet +** | 34 465.8 | 27 511.2 | 61 977 | 55.6% | |
| **Tet -** | 17 699 | 73 259 | 90 958 | 19.5% | 65% |

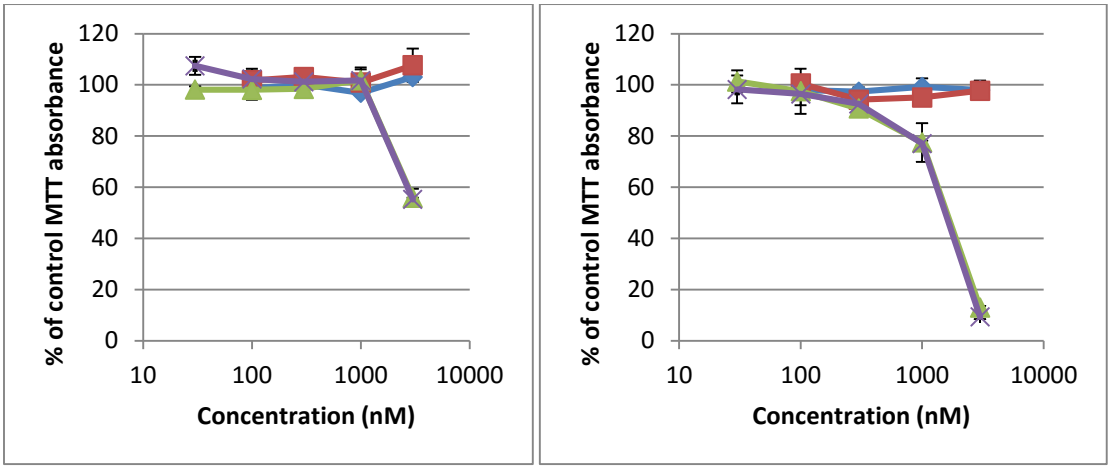


A




B

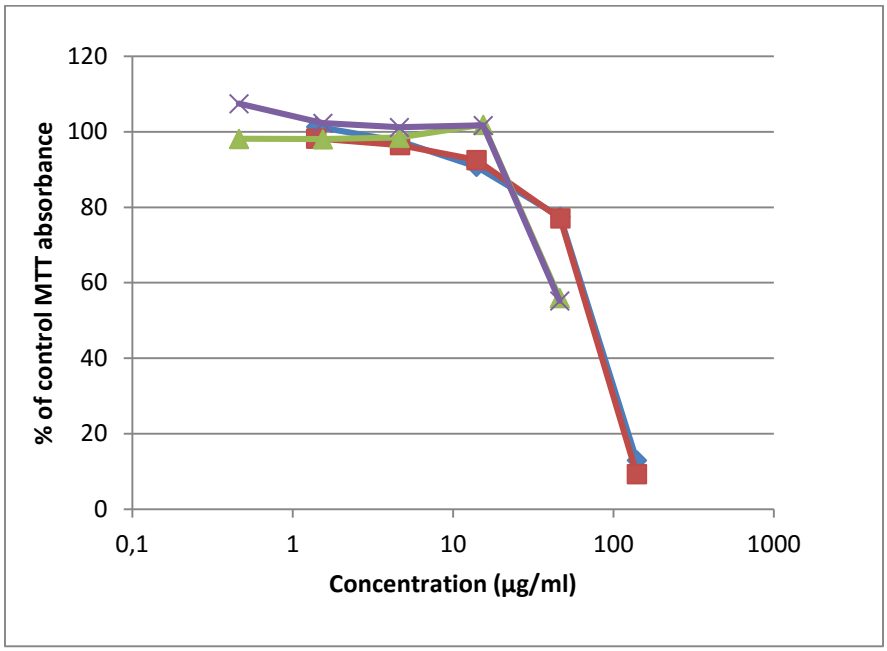


C

**Appendix Figure 2. Toxicity of cabazitaxel, docetaxel and loaded nanoparticles in Tet + and Tet - after 24 hours continuous incubation. A shows toxicity of cabazitaxel in Tet - (blue) and Tet + (red) and PIHCA+CTX in Tet - (green) and Tet + (purple). B shows toxicity of docetaxel in Tet - (blue) and Tet + (red) and PIHCA+DTX in Tet - (green) and Tet + (purple). C shows toxicity of the loaded nanoparticles, PIHCA+DTX in Tet - (blue) and Tet + (red) and PIHCA+CTX in Tet - (green) and Tet + (purple) showing their respective concentrations on nanoparticles.**

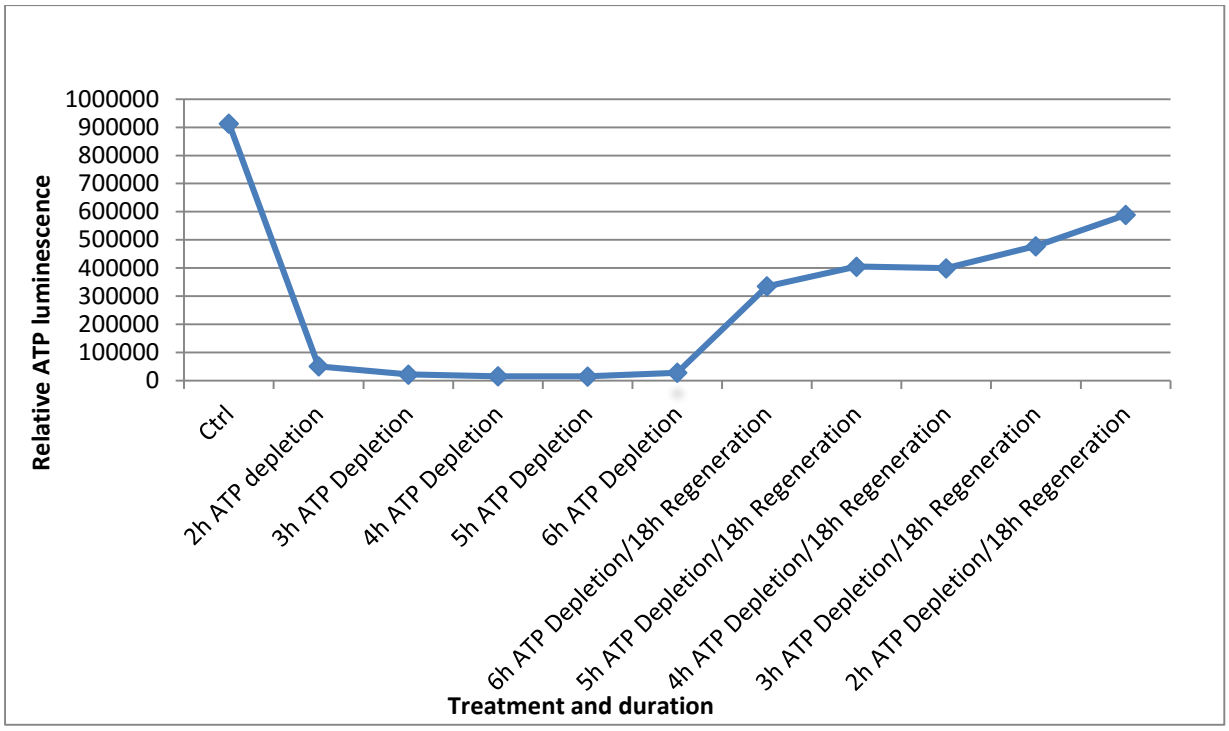


**Appendix Figure 3. HeLaP. ATP levels measured with CellTiter-Glo Assay after depletion with 10 mM Na-Azide and 6 mM 2-DG for 2, 3, 4, 5 and 6 hours with a subsequent 18 hour regeneration.**

**Appendix table 6. Reduction of endocytosis under effect of ATP depletion with 10 mM Na-Azide and 6 mM 2-DG in HeLaP.**

| Well | Pellet (cpm) | Supernatant (cpm) | Total (cpm) | % endocytosed | Reduction of endocytosis % |
|---|---|---|---|---|---|
| **Control** | 715.2 | 1 546.1 | 2 261.2 | 32 | |
| **1 hour** | 366.7 | 1 131.3 | 1 498 | 24 | 23 |
| **2 hour** | 221.8 | 876.4 | 1 098.2 | 20 | 36 |
| **3 hour** | 145.1 | 871.3 | 1 016.4 | 14 | 55 |

**Appendix table 7. Reduction of endocytosis under effects of inhibitors in MDA-MB-231.**

| Well/ Inhibitor | Pellet (cpm) | Supernatant (cpm) | Total (cpm) | % endocytosed | Reduction of endocytosis % |
|---|---|---|---|---|---|
| **Control** | 420 | 1 655.2 | 2 075.2 | 20.2% | |
| **CK-666** | 246.4 | 1 898.5 | 2 144.9 | 11.5% | 43.3% |
| **Dyngo** | 400 | 2 971.3 | 3 371.3 | 11.9% | 41.4% |
| **Latrunculin B** | 113.5 | 2 235.3 | 2 348.9 | 4.8% | 76.1% |